Role of ducting in relativistic electron loss by whistler-mode wave scattering

Anton V Artemyev, A. G Demekhov, X.-J -j Zhang, V. Angelopoulos, D. Mourenas, Yu V Fedorenko, J. Maninnen, E. Tsai, C. Wilkins, S. Kasahara, et al.

Role of ducting in relativistic electron loss by whistler-mode wave scattering

A. V. Artemyev[1,2], A. G. Demekhov[3,4], X.-J. Zhang [1], V. Angelopoulos[1], D. Mourenas[5], Yu. V. Fedorenko[3], J. Maninnen[6], E. Tsai[1], C. Wilkins[1], S. Kasahara[7], Y. Miyoshi[8], A. Matsuoka[9], Y. Kasahara[10], T. Mitani[11], Y. Shoichiro[12], K. Keika[7], T. Hori[8], S. Matsuda[11], S. Nakamura[8], M. Kitahara[8], T. Takashima[11], I. Shinohara[11]

[1]Department of Earth, Planetary, and Space Sciences, University of California, Los Angeles, USA
[2]Space Research Institute of Russian Academy of Sciences, Moscow, Russia
[3]Polar Geophysical Institute, Apatity, Russia
[4]Institute of Applied Physics, RAS, Nizhny Novgorod, Russia
[5]LPC2E, CNRS, Orleans, France
[6]Sodankylä Geophysical Observatory, Sodankylä, Finland
[7]Department of Earth and Planetary Science, School of Science, The University of Tokyo, Tokyo, Japan
[8]Institute for Space Earth Environmental Research, Nagoya University, Nagoya, Japan
[9]Graduate School of Science, Kyoto University, Kyoto, Japan
[10]Graduate School of Natural Science and Technology, Kanazawa University, Kakuma, Kanazawa, Japan
[11]Institute of Space and Astronautical Science, Japan Aerospace Exploration Agency, Sagamihara, 252-5210, Kanagawa, Japan
[12]Osaka University, Osaka, Japan

Key Points:

- Near-equatorial and ground-based measurements of whistler-mode waves are accompanied by relativistic electron precipitation
- In the presence (absence) of ducted wave propagation, as monitored by propagation to the ground, the precipitating electron energies are above (below) 150 keV
- Ducted whistler-mode waves may play a key role in relativistic electron loss in the inner magnetosphere

Corresponding author: Anton Artemyev, aartemyev@igpp.ucla.edu

Abstract

Resonant interactions of energetic electrons with electromagnetic whistler-mode waves (*whistlers*) contribute significantly to the dynamics of electron fluxes in Earth's outer radiation belt. At low geomagnetic latitudes these waves are very effective in pitch-angle scattering and precipitation into the ionosphere of low equatorial pitch-angle, tens of keV electrons and acceleration of high equatorial pitch-angle electrons to relativistic energies. Relativistic (hundreds of keV), electrons may also be precipitated by resonant interaction with whistlers, but this requires waves propagating quasi-parallel without significant intensity decrease to high latitudes where they can resonate with higher energy low equatorial pitch-angle electrons than at the equator. Wave propagation away from the equatorial source region in a non-uniform magnetic field leads to ray divergence from the originally field-aligned direction and efficient wave damping by Landau resonance with suprathermal electrons, reducing the wave ability to scatter electrons at high latitudes. However, wave propagation can become ducted along field-aligned density peaks (ducts), preventing ray divergence and wave damping. Such ducting may therefore result in significant relativistic electron precipitation. We present evidence that ducted whistlers efficiently precipitate relativistic electrons. We employ simultaneous near-equatorial and ground-based measurements of whistlers and low-altitude electron precipitation measurements by ELFIN CubeSat. We show that ducted waves (appearing on the ground) efficiently scatter relativistic electrons into the loss cone, contrary to non-ducted waves (absent on the ground) precipitating only < 150 keV electrons. Our results indicate that ducted whistlers may be quite significant for relativistic electron losses; they should be further studied statistically and possibly incorporated in radiation belt models.

1 Introduction

Relativistic electron fluxes in the Earths radiation belts are largely controlled by resonant interactions of such electrons with intense whistler-mode waves (*whistlers*) (Shprits et al., 2008; Thorne, 2010; Millan & Thorne, 2007; Millan & Baker, 2012; Kanekal & Miyoshi, 2021). When field-aligned, such waves are quite effective in accelerating electrons up to relativistic energies (Demekhov et al., 2006; Y. Chen et al., 2007; Thorne et al., 2013; Allison & Shprits, 2020). The most intense of these whistlers are lower-band chorus waves (Tsurutani & Smith, 1974). On the night-side, they are most frequently observed around the geomagnetic equator (Meredith et al., 2001, 2003; Agapitov et al., 2013, 2015) where they resonate with and accelerate near-equatorially mirroring (high pitch angle) electrons. On the dayside, however, these waves are often observed at middle geomagnetic latitudes (off the equator) (Meredith et al., 2012; Agapitov et al., 2013), where they can resonate with and scatter more field-aligned (small equatorial pitch angle) relativistic electrons toward the loss cone (Li et al., 2015; Agapitov et al., 2018; Wang & Shprits, 2019).

Resonant latitudes for field-aligned electrons rapidly increase with electron energy (Thorne et al., 2005; Shprits et al., 2006; Summers & Ni, 2008; Miyoshi et al., 2015). Therefore, scattering of relativistic electrons into the loss cone by field-aligned whistlers requires significant wave intensities above $|\lambda| \sim 30^\circ$ in geomagnetic latitude (Thorne et al., 2005; Summers et al., 2007; Miyoshi et al., 2020). Generated by plasma sheet electrons around the equator, and having an initially near field-aligned propagation (e.g., Fu et al. (2014)), whistler-mode lower band chorus waves travel away from the equator where their propagation direction diverges from the local magnetic field direction due to the plasma and field inhomogeneity (Kimura, 1985; Shklyar et al., 2004; Breuillard et al., 2012; Yamaguchi et al., 2013; Lu et al., 2019). Becoming oblique, they are damped due to Landau resonance with suprathermal electrons (Bortnik et al., 2006; L. Chen et al., 2013; Watt et al., 2013; Maxworth & Golkowski, 2017). Both the wave divergence and the damping imply low wave intensity at middle latitudes. Dayside chorus waves may reach $|\lambda| \sim 30^\circ$ due to the weaker dayside magnetic field inhomogeneity and the associated lower ray divergence and reduced wave damping (Tao et al., 2014), but their intensity still decreases and their obliquity increases with $|\lambda|$ (Agapitov et al., 2013, 2018; Santolík et al., 2014). Thus, although dayside waves can occasionally (during geomagnetically active times) attain wave-normal angles near the resonance cone and scatter ~ 1MeV electrons toward the loss cone (Agapitov et al., 2018; Artemyev et al., 2015, 2016; Mourenas, Artemyev, Agapitov, & Krasnoselskikh, 2014), the predominant low-intensity and mildly oblique character of dayside chorus renders it, on average, ineffective in relativistic electron scattering. Thus, up to now relativistic electron loss is typically attributed to two other mechanisms: magnetopause shadowing (Turner et al., 2012; Gao et al., 2015; Sorathia et al., 2017) or cyclotron resonance with electromagnetic ion cyclotron waves (Thorne & Kennel, 1971; Usanova et al., 2014; Blum et al., 2015; Ma et al., 2015; Mourenas et al., 2016; Shprits et al., 2016; Grach & Demekhov, 2020; Zhang et al., 2021).

However, in the presence of density ducts (in particular, density enhancements) which may develop due to plasmaspheric plumes, plasmapause density striations, ionospheric outflows or drift shell splitting and are confined within distinct flux tubes, chorus waves can be guided by diffraction and propagate to middle and high magnetospheric latitudes (far from the equator) while retaining their quasi-parallel propagation, and hence evade damping (Helliwell, 1965; Laird & Nunn, 1975). Indeed such ducting has been observed previously near strong plasma density gradients around the plasmapause (Inan & Bell, 1977; Woodroffe & Streltsov, 2013; R. Chen, Gao, Lu, Tsurutani, & Wang, 2021) and within large-scale plasmasphere plumes (Woodroffe et al., 2017; Li et al., 2019; Demekhov et al., 2017, 2020), but also near smaller scale structures (Hanzelka & Santolík, 2019; Streltsov & Bengtson, 2020; Hosseini et al., 2021; R. Chen, Gao, Lu, Chen, et al., 2021; Ke et al., 2021) which can be formed by compressional ultra-low-frequency waves or localized ionospheric outflows (Artemyev et al., 2020). Ducted chorus waves surviving with large amplitude and low obliquity at middle latitudes (off the equator), can potentially provide effective scattering of relativistic electrons as evidenced by modeling (L. Chen et al., 2020; Miyoshi et al., 2020, 2021). To prove that this type of relativistic electron scattering and precipitation by whistlers actually occurs, it is not sufficient to observe the waves and relativistic electrons at the equator: it also requires confirmation that the waves are ducted, as evidenced by ground-based wave receivers (Manninen et al., 2013; Martinez-Calderon et al., 2015; Shiokawa et al., 2017), and that the relativistic electrons are precipitating, as measured at the ionosphere above the ground station. Both ground receivers and ionospheric measurements of precipitation need to be in good magnetic conjunction with the near-equatorial wave and electron measurements. On the one hand, if a good correlation between ground-observed whistlers with those at the equator is found (Titova et al., 2015, 2017; Demekhov et al., 2020; Martinez-Calderon et al., 2016, 2020) this can prove ducted propagation, as this is the only way that equatorial whistlers can survive damping and appear on the ground. On the other hand, if we can employ simultaneous low-altitude (ionospheric) measurements of electron precipitation, which is well correlated with equatorial whistler-mode waves (Li et al., 2013; Li, Mourenas, et al., 2014; Ni et al., 2014), then the energy range of that precipitation can be used to determine whether scattering by ducted whistler is occurring. If precipitation of relativistic electrons is well-correlated with both ground and equatorial whistlers, this would confirm that ducting occurs and relativistic electron precipitation by ducted whistlers also takes place. If precipitation of only non-relativistic electrons is occurring in good correlation with equatorial whistlers but in the absence of whistlers on the ground (no ducting) this would also confirm the converse: that in the absence of wave ducting relativistic scattering (expected only by ducted whistlers) does not occur, but sub-relativistic scattering (due to equatorial whistlers) does occur, as expected from prior studies (Nishimura et al., 2010; Li et al., 2013; Li, Mourenas, et al., 2014; Ni et al., 2014; S. Kasahara, Miyoshi, et al., 2018).

In this paper we set out to examine this hypothesis. We combine the following datasets: (i) near-equatorial measurements of whistlers and of fluxes of relativistic electrons using Time History of Events and Macroscale Interactions during Substorms (THEMIS; Angelopoulos (2008)) and Exploration of energization and Radiation in Geospace (ERG; Miyoshi, Shinohara, Takashima, et al. (2018)) spacecraft; (ii) ground measurements of Very Low Frequency (VLF) waves revealing presence or absence of whistlers (bespeaking of ducted wave propagation to high latitudes, or of damping, respectively) using stations Lovozero (Fedorenko et al., 2014) and Kannuslehto (Manninen et al., 2013); and (iii) low-altitude ($\sim$400 km) measurements of energetic electron precipitation spectra, revealing relativistic or sub-relativistic precipitation (implying electron scattering at middle latitudes or low-latitudes, respectively) by ELFIN (Angelopoulos et al., 2020).

We first describe the datasets and instruments used (Sect. 2). We then present the four selected conjunction events (Sects. 3.1-3.3). We discuss our findings in Sect. 4. Of the four events, the first two show ducted whistlers concurrent with relativistic electron precipitation, whereas the other two show the absence of both ducting and precipitation. The first event (Sect. 3.1) includes equatorial THEMIS observations of whistlers modulated by compressional ultra-low-frequency (ULF) oscillations extending from the vicinity of the flank magnetopause to the plasmapause. Ground VLF receivers, in conjunction with these space observations, showed VLF emissions demonstrating ducted propagation of whistler waves in the magnetosphere, demonstrating their ducted propagation. Simultaneous ELFIN observations confirm precipitation of 700 keV electrons. The second event (Sect. 3.2) shows similar evidence of relativistic electron precipitation and ducting as the first event, except that the near-equatorial whistlers are measured by ERG. The last two events comprise measurements from similar ground and space conjunctions as the second event, but show an absence of both ground whistlers and relativistic electron precipitation, demonstrating that the lack of ducting correlates with a lack of relativistic electron scattering (see Sect. 3.3). These events do show sub-relativistic precipitation, consistent with pitch-angle scattering of $<$ 150keV by equatorial whistlers. Accordingly, we hereafter use $\sim$ 150 keV as the threshold energy separating two events with relativistic electron precipitation (up to 700 keV) and non-relativistic (below 150 keV) electron precipitation. Note that although ground-based measurements of whistler waves are not rare, available ground-based conjugations with equatorial whistler measurements are limited to several good examples (Titova et al., 2015, 2017; Demekhov et al., 2020; Martinez-Calderon et al., 2016, 2020). The additional requirement of a conjugation of ground-based and equatorial observations with ELFIN low-altitude measurements of precipitations further reduces significantly the number of events. As a consequence, the results of the present study are based on only four events and should be considered (in addition to the results of recent simulations, see L. Chen et al. (2020, 2021); Namekawa et al. (2021)) as an observational indication of the possibly important role of whistler-mode wave ducting for relativistic electron precipitations.

2 Datasets

In the first event the near-equatorial measurements are provided by THEMIS D and A (Angelopoulos, 2008). We use spin resolution (3 second) measurements of the background magnetic field by the fluxgate magnetometer (Auster et al., 2008), fluxes and anisotropies for <25 keV electrons by the electrostatic analyzer (McFadden et al., 2008), and fluxes for $50-500$ keV electrons by the solid state telescope (Angelopoulos et al., 2008). Wave magnetic measurements of 10–4000 Hz Nyquist by the search-coil magnetometer (Le Contel et al., 2008) are also shown. During the first event there are no Fast Survey mode wave captures onboard THEMIS A, the closest to the ground-based VLF receivers, so wave observations are limited to spin-resolution spectra at six broad frequency bands (Cully, Ergun, et al., 2008).

In the other three events the near-equatorial measurements are provided by ERG/Arase (Miyoshi, Shinohara, Takashima, et al., 2018). We use measurements of the magnetic field investigation (Matsuoka, Teramoto, Nomura, et al., 2018) at 8 second resolution, high-energy electron fluxes from the Medium-energy particle experiments-electron analyzer (S. Kasahara, Yokota, Mitani, et al., 2018) ($7-100$ keV) and from the High-energy electron experiments (Mitani, Takashima, et al., 2018) ($70-1000$ keV), both at 16 second resolution. We also used 1s resolution electric and magnetic field wave spectra collected by the onboard frequency analyzer (Matsuda et al., 2018) of the Plasma wave instrument (Y. Kasahara, Kasaba, et al., 2018).

For ground magnetic measurements of waves in the $0.2-16$ kHz range, corresponding to equatorial whistlers, we used receivers at Kannuslehto (KAN) in northern Finland (67.74°N, 26.27°E; $L_{IGRF}\sim5.51$; see Manninen et al. (2013, 2014)), and at Lovozero (LOZ) in northern Russia (67.98°N, 35.08°E; $L_{IGRF}\sim5.54$; see Fedorenko et al. (2014); Demekhov et al. (2020)).

Our energetic electron precipitation measurements were collected by the ELFIN CubeSats, at $\sim$440 km altitude (Angelopoulos et al., 2020). Their energetic electron detector measures electrons between 50 keV to 5 MeV energy with energy resolution $\Delta E/E \leq 40\%$. The entire 180° range of pitch-angles can be covered twice every 3 seconds, the ELFIN spin period. In this study we use full time and energy resolution spectra of fluxes, pitch-angle averaged either within the local loss cone j_{loss} or outside it and its supplement (trapped or quasi-trapped), j_{trap}.

For all events in our study, we also used measurements from NOAA spacecraft on polar, low-altitude orbits from the same MLT and L-shell region as ELFIN. We use j_{loss}/j_{trap} from the >30 keV energy channel of NOAA spacecraft as a proxy of equatorial whistler-mode wave activity (see Li et al. (2013); Ni et al. (2014)).

Figure 1. Overview of THEMIS A observations during the first event: electron cyclotron and plasma frequencies, and spacecraft L-shell calculated using the T96 model (Tsyganenko, 1995) (a), square root of intensity of wave magnetic and electric fields in the frequency range $250 - 750$ Hz, after spin-period (3s) time-averaging (b), electron phase space density omni-directional energy-spectrogram (c), flux anisotropy of $<$ 20keV electron population (d), compressional magnetic field fluctuations with frequencies >0.1 Hz (red) and >0.01 Hz (black) (e).

3 Analysis of observations

3.1 Event #1

Figure 1 shows an overview of THEMIS A observations during an inbound section of its orbit (from high to low L-shells) on 29 September 2019. A localized density enhancement (inferred from the spacecraft potential measurements and presented in units of plasma frequency in panel (a)) is seen at 14:30-15:20 UT). It is evidence of transient crossing of the plasmasphere or a narrow plasma plume. Prior to it (between 12:00-14:30 UT) and right after it (15:20 - 17:00 UT) THEMIS A was in the lower plasma density outer radiation belt. During these two time intervals, THEMIS A detected sporadic whistler emissions (panel (b)): peaks of magnetic (black) and electric (red) wave intensity between $\sim 250 - 750$ Hz (i.e., at $\sim$ $0.1 f_{ce}$ to $0.6 f_{ce}$; f_{ce} is depicted in panel (a)). As THEMIS A was in Slow Survey mode at the time, only the fbk dataset of wave spectra is available (Cully, Ergun, et al., 2008). This fbk dataset is mostly used for the determination of wave presence. However, Cully, Bonnell, and Ergun (2008) have shown that wave amplitudes provided by fbk, which are averaged over a long $\sim 3-4$ second interval, can underestimate whistler-mode chorus wave-packet amplitudes by a factor of $\sim 20-30$. A comparison of wave amplitudes from fbk and fff measurements on THEMIS D during this period indeed shows that wave amplitudes from fff are a factor of ~ 30 higher than 4-second time-averaged amplitudes from fbk (see Fig. 1 in SI; the same figure further shows that the cB/E wave ratio from the fff dataset is close to the expected magnitude of the whistler-mode refractive index for the observed plasma frequency and cyclotron frequency). Accordingly, the real peak amplitudes of wave-packets during this event are probably higher by a similar factor ~ 30 than time-averaged values from fbk, corresponding to $\sim 100 - 200$ pT. Such wave amplitudes are sufficiently high to provide a strong (potentially non-linear) scattering of $50-300$ keV electrons at $L>6$ (Tao & Bortnik, 2010; Artemyev et al., 2016; Zhang, Mourenas, et al., 2019), leading to a significant electron precipitation.

The phase space density of energetic (50–500 keV) electrons, seen in panel (c), increases toward lower L-shells (higher f_{ce}). The phase space density of thermal electrons (tens of eV to $<$ 25 keV), also in panel (c), shows a quasi-periodic variations in the interval prior to the transient plasmasphere/plume encounter. The subset of thermal electrons between 6 keV to 20 keV shows distinct and persistent transverse anisotropy that is the free energy source (Trakhtengerts, 1963; Kennel & Petschek, 1966) for the observed whistlers (panel (d)). As THEMIS A was in Slow Survey mode at the time, the available time resolution of the anisotropy product, $\sim$ 5min, is too slow to allow examination of the correlation of the anisotropy with the wave power. The parallel component of the background magnetic field shows compressional ULF waves (panel (e)) that are likely responsible for the modulation of the thermal electron fluxes. Such modulation of flux and flux anisotropy by compressional ULF waves has been previously linked to whistler wave power modulation (e.g., Zhang, Chen, et al. (2019)) and it is the likely explanation of the whistler wave power modulation in this event too.

While THEMIS A captured the above measurements near the dusk terminator, THEMIS D moved from low to high L-shells near noon, crossing the plasmapause at around 13:15 UT (Fig. 2(a)). At 17:30 UT THEMIS D crossed the magnetopause and left the magnetosphere (not shown). The plasmapause was encountered at $L \sim 3.5$, consistent with the expected plasmapause location $L_{pp} \simeq 3.6 \pm 0.6$ from a statistical model (O'Brien & Moldwin, 2003) for $\max(K_p) = 4.7$ during the preceding 36 hours. Search-coil measurements of the whistler spectrum at high spectral and temporal resolution and electron anisotropy

Figure 2. Overview of THEMIS D observations during the first event: electron cyclotron and plasma frequencies, and spacecraft L-shell calculated using the T96 model (Tsyganenko, 1995) (a), high-resolution magnetic field spectrogram (available only after 14:50 UT) (b), electron phase space density omni-directional energy-spectrogram (c), flux anisotropy of < 20 keV electron population (d), compressional magnetic field variations with frequencies > 0.1 Hz (red) and > 0.01 Hz (black) (e).

Figure 3. Projections of THEMIS A, THEMIS D, METOP 1, NOAA 19, and two ELFIN A orbits to the north hemisphere for the time interval of the first event. Colors in the projections of the low altitude spacecraft (all but THEMIS) denote the ratio of precipitating to trapped electron fluxes (for scaling convenience we show the square root of the flux ratio instead). Ground stations LOZ and KAN, equipped with receivers able to detect whistlers waves, are shown by blue dots. Dotted red lines show L-shells calculated using the T96 model (Tsyganenko, 1995).

Figure 4. Electron fluxes within the loss cone and ratio of precipitating to trapped fluxes from the >30 keV integral channel of NOAA 19 and METOP 1 low-altitude spacecraft. L-shells of spacecraft projections to the equatorial plane with the T96 (Tsyganenko, 1995) model are shown in grey.

measurements are available during the second half of this interval, at $L > 6$, when the data collections were operated in Fast Survey mode. During that time, THEMIS D observations (Fig. 2) are similar to those at THEMIS A in the same L-shell range. Specifically, the intense compressional ULF waves (panel (e)) likely responsible for the observed modulation of the thermal electron fluxes (panel (c)) and of the $\sim 400 - 1000$ Hz ($f \sim 0.2$ to 0.5 f_{ce}) whistlers (panel (b)) are all observed. The intense transverse anisotropy of < 20 keV electrons is also present on THEMIS D, as it was on THEMIS A. The similarity of the measurements at THEMIS A and D shows that ULF-modulated whistlers cover a wide range of MLTs (from 11 to 18) and L-shells (from ~ 4 to 11) outside the plasmasphere during this time.

During this interval, THEMIS A's footpoint was north of Scandinavia (Fig. 3) whereas THEMIS D's was in the south of Greenland. ELFIN A's projections and those of two NOAA spacecraft were also in the vicinity. Given the aforementioned, concurrent THEMIS A and D detection of whistlers over a broad MLT and L-shell range, the MLT sector between Greenland and Scandinavia is expected to be replete with electron precipitation driven by ULF-modulated equatorial whistlers. To examine this hypothesis, low altitude spacecraft projections have been colored according to the square root of the ratio of precipitating to trapped electron fluxes (for > 50 keV or > 30 keV electrons on ELFIN or NOAA spacecraft respectively). The displayed orbits of NOAA spacecraft MetOp 1 and NOAA 19 are within the time interval of THEMIS A observations of whistlers; the high level of electron precipitation observed by MetOp 1 at $L > 6$ bespeaks intense equatorial whistler activity. Indeed, Figure 4 shows moderate > 30 keV electron precipitations with j_{loss}/j_{trap} reaching ~ 0.1 at higher L-shells at MetOp 1. NOAA 19 observations correspond to lower L-shells, and NOAA 19 detected several peaks of precipitations with $j_{loss}/j_{trap} \sim 0.1$ only when it reached $L \sim 7 - 8$ (see Fig. 4). These precipitations at $L > 6$ have a transient nature that could be due to the temporal or spatial quasi-periodicity of the whistlers. The ULF-modulated electron anisotropy is expected to generate equatorial whistlers with some periodicity in both time and space (see Motoba et al. (2013); Zhang et al. (2020)). This hypothesis is consistent with ELFIN A, METOP 1 and NOAA 19 observations of tens of keV electron precipitation from a broad MLT and L-shell region (see Fig. 3).

Figure 5 shows spectra of trapped and precipitating electrons measured by ELFIN A between 13:23-13:27 UT. Precipitating fluxes reach relativistic energies of 700 keV. Over the entire energy range, precipitating fluxes show successive enhancements and decreases. The transient nature of precipitation may be due to the spatio-temporal localization of whistlers

Figure 5. Trapped and precipitating electron fluxes measured during the first ELFIN A orbit (13:23-13:27 UT) of the first event. The L-shell computed using the T96 model (Tsyganenko, 1995) is also shown in black.

Figure 6. Trapped and precipitating electron fluxes measured during the second ELFIN A orbit (14:55-15:00 UT) of the first event. The L-shell computed using the T96 model (Tsyganenko, 1995) is also shown in black.

Figure 7. Minimum resonant energy (in keV) for field-aligned electrons as a function of resonant latitude and equatorial whistler-mode wave frequency. The three panels depict three different f_{pe}/f_{ce} equatorial values, around the most probable value $f_{pe}/f_{ce} = 6$ (based on THEMIS equatorial measurements) during the ELFIN A observations of 700 keV electron precipitation. Top panels show estimates for a constant plasma density independent of magnetic latitude λ, and bottom panels show estimates for a plasma density variation $\sim \cos^{-5}(\lambda)$ based on the model from Denton et al. (2006).

as they are modulated by ULF waves, consistent with equatorial observations at THEMIS A and D. The losses of such high energy electrons by quasi-parallel whistlers would require electron cyclotron resonant scattering at middle latitudes. Figure 7 shows the typical latitudes of cyclotron resonance between quasi-parallel whistler-mode waves and low equatorial pitch-angle electrons for different electron energies. Equatorial THEMIS D measurements at 13:25-14:15 UT (see Figure 2(a)) on the same $L-$shells as ELFIN A imply that $f_{pe}/f_{ce} \sim 6$ during ELFIN A observations of relativistic electron precipitation near 13:25 UT. Taking into account that whistlers measured by THEMIS D at 14:50-15:30 UT have relatively stable normalized frequencies $f/f_{ce} \sim 0.2-0.3$, the latitude of cyclotron resonance with the observed 700 keV precipitating electrons can be estimated as $\sim 30^\circ$. These are quite high latitudes for whistlers, whose wave intensity should be significantly decreased by wave divergence and Landau damping in the absence of ducting (Breuillard et al., 2012; Agapitov et al., 2013; Watt et al., 2013; L. Chen et al., 2013). Therefore, we expect that the whistlers providing scattering of these relativistic electrons are likely ducted during this event. Note that for $f_{pe}/f_{ce} \sim 6$, cyclotron resonance with typical electromagnetic ion cyclotron waves only occurs for electron energies much higher than 1 MeV (Summers & Thorne, 2003; Kersten et al., 2014), implying that the observed precipitations of < 700 keV electrons are most probably related to electron scattering by whistlers.

The next ELFIN A orbit (at 14:55-15:00 UT) is closer to THEMIS D (see Fig. 3) and covers lower L-shells in comparison with the first orbit. Figure 6 shows the corresponding ELFIN measurements of trapped and precipitating electron fluxes. There is a quite clear boundary to the domain of high electron flux near $L \sim 4$, which agrees well with both the plasmapause position observed by THEMIS D and the plasmapause location predicted by statistical models (O'Brien & Moldwin, 2003). At higher L-shells, ELFIN A measured precipitating fluxes of relativistic electrons up to 700 keV, in agreement with measurements performed during the previous orbit (compare Figs. 5 and 6).

Ground measurements confirm our expectation that whistlers propagate to high geomagnetic latitudes (lower altitudes) and down to the ground due to ducting during this event. Figures 8, 9 show one hour of measurements at LOZ and KAN between 13 UT and 14 UT (bottom two panels in each figure are expanded views of two 10 min intervals). Both stations are at $L \sim 6.2$, near the THEMIS A and NOAA19 footpoints. Quasi-periodic emissions are evident over the entire frequency range, [500,2000] Hz. The periods of these wave amplitude modulations vary from ~ 30 seconds in the beginning of the hour to > 3 min at the end of the hour. Comparison of the wave power spectral density in the expanded-view spectrograms with the superimposed $\delta B_\parallel$ ULF variations from THEMIS A confirm that the two quantities have a similar periodicity (which is also similar to the periodicity seen by THEMIS D as discussed above). We also compare the spectrum of ULF $\delta B_\parallel$ and the

Figure 8. One hour (top panel) of VLF wave spectrogram measured at LOZ. The two bottom panels show spectrogram expanded views, each of 10 min in duration, together with compressional magnetic field variations measured at THEMIS A (black curves).

Figure 9. One hour (top panel) of spectrograms of VLF measured at KAN. Two bottom panels show spectrogram expanded views, each of 10 min duration, together with compressional magnetic field variations measured at THEMIS A (black curves).

Figure 10. Overview of ERG observations during the second event: electron number flux in two different energy ranges (a,b), wave electric and magnetic field spectra in the whistler-mode frequency range (c,d), spacecraft L-shell calculated using the T96 model (Tsyganenko, 1995) (e). White curves on panels (c,d) show 1/2 and 1/10 of the local electron gyrofrequency f_{ce}.

Figure 11. Projections of ERG, METOP 1,2, NOAA 19, 18, and 15, and ELFIN A orbits to the north hemisphere for the time interval of the second event. Colors in the projections of the low altitude spacecraft (all but ERG) denote the ratio of precipitating to trapped electron fluxes (for scaling convenience we show the square root of the flux ratio instead). Locations of LOZ and KAN ground-based stations measuring VLF waves are depicted as blue dots.

spectrum of frequency averaged ($1-1.75$kHz) ground-based wave power: both spectra show a strong peak around a ~ 2 min periodicity (see Fig. 2 in SI). Therefore, the ULF-wave modulated whistlers observed near the equator at THEMIS A and D over a wide (L,MLT) range are probably ducted so as to propagate to the ground during this event. Such ducted wave propagation would allow resonant electron scattering at middle latitudes, explaining ELFIN A's measurements of intense precipitation of relativistic electrons at MLTs between those of the THEMIS A and D footpoints.

3.2 Event #2

Near-equatorial observations during the second event, which occurred on the day after the first, were obtained by ERG (Figure 10). As ERG was moving towards lower L-shells, around 04:30 UT (when L was below 6 and $|\lambda|>20^\circ$) it started observing whistler waves with frequencies >1 kHz ($\sim(0.1{-}0.2)f_{ce}$). Based on statistical plasmapause models parameterized by Kp (O'Brien & Moldwin, 2003), the plasmapause was likely at $L_{pp}\sim 3.5-4$ at the time, much closer to Earth than ERG's location. The observed whistler-mode waves are grouped into bursts of $\sim 10-30$ s duration each. The temporal increase of observed wave frequencies is likely a spatial effect, i.e. higher-frequency waves were probably present at $L<5$ even before 05:00 UT, and were only observed by ERG when it reached this lower L-shell range. During the decrease of L along ERG orbit, electron <50 keV fluxes decreased, but relativistic (>500 keV) electron flux increased. ERG's footpoint in the north hemisphere was near ground stations measuring whistler-mode waves (see Fig. 11). During ERG's observations of whistlers, several passes of NOAA and METOP low-altitude spacecraft took place. The precipitating to trapped flux ratio for >30 keV electrons on these spacecraft bespeaks of the presence of intense whistlers at the equator that are able to scatter electrons of this energy (see colors on Fig. 11). Figure 12 shows >30 keV electron precipitating fluxes and precipitating-to-trapped flux ratios from NOAA-19 and METOP-1. Strong precipitation and high precipitating to trapped flux ratio for L-shells above 4 was seen at both satellites. Similarly, large precipitating to trapped flux ratios are observed on ELFIN A, although its orbit is projected at a fairly large MLT distance from ERG.

Figure 13 shows spectra of precipitating and trapped electrons measured by ELFIN A (note there are several blank intervals without measurements). The strong bursts of

Figure 12. Electron fluxes within the loss cone and ratio of precipitating to trapped fluxes from the $>$ 30 keV integral channel of NOAA 19 and METOP 1 spacecraft. L-shells obtained by using the T96 model (Tsyganenko, 1995) are shown in grey.

Figure 13. Trapped and precipitating electron fluxes measured by ELFIN A during the second event. L-shell of spacecraft projection to the equatorial plane with the T96 model (Tsyganenko, 1995) is shown in black.

Figure 14. One hour (top panel) of chorus wave intensity measurements at LOZ. Two bottom panels show expanded views of 10 min duration.

precipitation around $L \sim 6$ and $L \sim 7$ are consistent with NOAA-19 and METOP 1 measurements at high L-shells (see Fig. 12). The precipitation of relativistic > 500 keV electrons is significant down to $L \sim 5$, and the precipitating flux is comparable to the trapped flux. During this event, whistlers had normalized frequencies $f/f_{ce} \sim 0.1 - 0.2$ and f_{pe}/f_{ce} was likely $\sim 5 - 10$ based on both a statistical plasma trough density model (Sheeley et al., 2001) and measurements obtained by THEMIS A and D at the same L-shells on the previous day (see Fig. 1,2). Thus, the strong precipitation observed is likely due to ducted whistlers propagating to middle latitudes (see Fig. 7). Electron resonant scattering by typical electromagnetic ion cyclotron waves (Kersten et al., 2014) can be excluded from consideration, because for $f_{pe}/f_{ce} \sim 5 - 10$ the energies of cyclotron resonant electrons then well exceed 1 MeV (Summers & Thorne, 2003; Kersten et al., 2014).

Indeed, ground observations at LOZ between 4:00-5:00 UT (Figure 14) show intense, bursty waves at $\sim 1 - 2$ kHz, of a nature and frequency similar to that of the waves observed at ERG after 4:45 UT (~ 2 kHz, Figure 10). Low-frequency ~ 1 kHz waves observed by ERG are also seen at LOZ, but they are partially blurred by noise. Therefore, Figs. 10, 13, and 14 show a consistent picture of whistlers generated around the equator, then ducted and propagating down to the ground, after having scattered relativistic electrons at middle latitudes. However, this event is less clear than the first one, due to the larger MLT separation of the equatorial ERG and low-altitude ELFIN A spacecraft, and due to several gaps in ELFIN A measurements at low L.

3.3 Events #3&4

These two events are characterized by ERG-ELFIN-LOZ conjunctions, but without relativistic electron precipitation on ELFIN A and without ground-based measurements of whistler-mode waves. Therefore, we consider these events as additional confirmation of the importance of whistler ducting for relativistic electron scattering.

Figures 15 and 16 show projections of ERG, ELFIN A and NOAA spacecraft orbits to the north hemisphere, with colors denoting the precipitating to trapped flux ratio of ≥ 30 keV electrons (except for ELFIN A for which ≥ 50 keV electron fluxes are used). These flux ratios are known to be positively correlated with the level of whistler wave activity near the equator (Li et al., 2013; Li, Mourenas, et al., 2014; Ni et al., 2014). The conjugate, equatorial ERG measurements for these two events show much lower intensity waves than for events #1,2. During event #3, ERG was around the equator ($|\lambda| < 15^\circ$) and observed whistlers at ~ 1 kHz, but with very weak magnetic field intensity and a strong electric field intensity (indicating they were very oblique, see Artemyev et al. (2016)). Such oblique waves usually experience strong Landau damping and, thus, often cannot reach middle latitudes to scatter energetic electrons (Bortnik et al., 2007; L. Chen et al., 2013), although a small population of these waves can sometimes be observed up to $\lambda \sim 45^\circ$ on the dayside when $Kp < 5$ (Agapitov et al., 2018). During event #4, ERG was quite far from the equator ($|\lambda| > 25^\circ$) and did not measure any wave power in the whistler frequency range, but only hiss-like emissions, below 1 kHz. During both events the ground-based receiver at LOZ, conjunct to the above

Figure 15. Projections of ERG, NOAA 15 and 18, and ELFIN A orbits to the north hemisphere for the time interval of the third event. Colors in the projections of the low altitude spacecraft (all but ERG) denote the ratio of precipitating to trapped electron fluxes (for scaling convenience we show the square root of the flux ratio instead). Locations of LOZ and KAN ground-based stations measuring VLF waves are depicted as blue dots.

Figure 16. Projections of ERG, NOAA 15 and 19, and ELFIN A orbits to the north hemisphere for the time interval of the fourth event. Colors in the projections of the low altitude spacecraft (all but ERG) denote the ratio of precipitating to trapped electron fluxes (for scaling convenience we show the square root of the flux ratio instead). Locations of LOZ and KAN ground-based stations measuring VLF waves are depicted as blue dots.

Figure 17. Trapped and precipitating electron fluxes measured by ELFIN A during the third event. L-shell of spacecraft projection to the equatorial plane with the T96 model (Tsyganenko, 1995) is shown in black.

Figure 18. Trapped and precipitating electron fluxes measured by ELFIN A during the fourth event. L-shell of spacecraft projection to the equatorial plane with the T96 model (Tsyganenko, 1995) is shown in black.

space measurements, also did not show any significant VLF wave power, confirming ERG's observations of the absence of intense quasi-parallel waves that may propagate far from the equator without being strongly damped (see ERG and ground-based observations in the Supplementary Material).

ELFIN A measurements of trapped and precipitating electron fluxes during events #3, 4 are shown in Figs. 17 and 18. For both events, trapped fluxes remain quite high up to 500 keV (especially at higher L-shells), whereas precipitating fluxes reach a measurable level only below $\sim$150 keV. Electrons of such low energies can be efficiently scattered around the equatorial plane (see Fig. 7 for resonant latitudes), and the absence of precipitation of $>$300 keV electrons suggests the absence of whistler waves at middle latitudes. Therefore, ELFIN A measurements confirm that in the absence of chorus wave propagation to middle latitudes, there is often no loss of relativistic electrons.

4 Discussion and conclusions

In this study, we show that observations of relativistic electron precipitation at the low-altitude ELFIN CubeSat are associated with observations of ducted whistlers propagating from their equatorial source region down to ground-based stations. Such ducted waves are, in fact, often observed on the ground (see statistics in Spasojevic (2014); Martinez-Calderon et al. (2015)) and have been analyzed in detail for several good conjunctions with equatorial spacecraft (Titova et al., 2017; Demekhov et al., 2020; Martinez-Calderon et al., 2016). However, there is presently no statistical analysis of the occurrence rate of this ducted wave population, i.e., there is no well justified approach on how to separate ducted from non-ducted waves captured by near-equatorial spacecraft for including the distinct ducted wave population and its important, relativistic scattering effects into radiation belt models. Empirical chorus wave models typically provide time-averaged wave statistics (Agapitov et al., 2018; Meredith et al., 2012; Wang et al., 2019) that include a mixture of ducted and non-ducted waves at middle latitudes ($>25^\circ$) (Agapitov et al., 2015, 2018) – or only consider low latitude ($<20^\circ$) waves (Wang et al., 2019).

However, it is worth noting that the comprehensive lower-band chorus wave model developed by Agapitov et al. (2018), using combined Van Allen Probes and Cluster data, does include separate contributions from quasi-parallel and very oblique waves. It shows that most of the magnetic wave power measured at latitudes $\lambda \sim 25^\circ - 40^\circ$ indeed corresponds to quasi-parallel waves (see Figure 10 from Agapitov et al. (2018)), which are likely ducted waves (Artemyev et al., 2016; Ke et al., 2021), since they have not been diffracted as significantly as expected in an inhomogeneous magnetic field in the absence of ducts. The largely dominant ducted chorus wave power can be obtained as a function of latitude, L, MLT, and Kp, by multiplying the total wave power B_w^2 from equation (2) in Agapitov et al. (2018) by the fraction of field-aligned wave power derived from their equation (4). This presumably ducted chorus wave power is larger in the $4-20$ MLT sector and when $Kp \sim 1-5$ (Agapitov et al., 2018), consistent with events #1 and #2.

There are two possible approaches for a more direct quantification of the ducted wave population. The first consists of a statistical comparison of ground-based and near-equatorial wave measurements. Modern networks of ground-based stations for whistlers include tens of stations (Shiokawa et al., 2014; Manninen et al., 2013; Fedorenko et al., 2014; Shiokawa et al., 2017; Ghaffari et al., 2020) with good MLT coverage. Studies of conjunctions between these stations and near-equatorial spacecraft Van Allen Probes (Demekhov et al., 2020) and ERG (Martinez-Calderon et al., 2020) missions have had good success in demonstrating that wave ray propagation to the ground indeed occurs. Therefore, time-, activity- and MLT- or L-shell-weighted statistics of whistlers measured simultaneously on the ground and at spacecraft in conjunction with the ground stations could potentially determine the wave ducting occurrence rate as a function of geomagnetic activity, MLT and L-shell. The second approach consists of statistical investigations of the conditions favorable for wave ducting. Various ray-tracing simulations have determined the magnitude of plasma density fluctuations necessary for ducting of whistler-mode waves (Hanzelka & Santolík, 2019; Streltsov & Bengtson, 2020; Hosseini et al., 2021; R. Chen, Gao, Lu, Chen, et al., 2021; Ke et al., 2021). Moreover, the plasma density distribution and dynamics in the inner magnetosphere has been recently parameterized in great detail via machine-learning models (Chu et al., 2017; Zhelavskaya et al., 2017). A combination of such detailed plasma density models and massive ray-tracing simulations may permit determination of the ducted wave occurrence rate. The obtained occurrence rates could finally be compared with the statistical distributions of chorus wave-normal angles obtained from Cluster observations at middle to high latitudes (Agapitov et al., 2015, 2018).

Whistler-mode chorus waves in the Earth's radiation belts may accelerate electrons to relativistic (Miyoshi et al., 2003; Demekhov et al., 2006; Li, Thorne, et al., 2014; Mourenas, Artemyev, Agapitov, Krasnoselskikh, & Li, 2014) and even ultra-relativistic (Allison & Shprits, 2020; Thorne et al., 2013) energies, but the same waves may be responsible for electron losses due to scattering into the loss cone. As we show in this study, scattering of relativistic electrons would be much more effective for ducted whistlers, whereas such ducting is generally associated with local plasma density enhancements (Karpman & Kaufman, 1982; Pasmanik & Trakhtengerts, 2005). Interestingly, the most effective electron acceleration by whistlers is associated with plasma density depletions (Thorne et al., 2013; Agapitov et al., 2019; Allison et al., 2021; Summers et al., 1998). Therefore, the regime of electron interaction with whistlers may be controlled also by the spatial distribution of plasma density, and this significantly increases the importance of developing more realistic plasma density models (Chu et al., 2017; Zhelavskaya et al., 2017; Goldstein et al., 2019).

To conclude, we have considered four events with conjugate observations of equatorial whistler-mode waves, ground-based chorus waves, and precipitating electrons on the low-altitude ELFIN A CubeSat. The main results are as follows:

1. During the first event on 2019-09-29 at 12:00-15:00 UT, near-equatorial THEMIS A and D spacecraft observed intense ultra-low-frequency compressional waves with typical timescales of $\delta B_\parallel$ fluctuations of about $0.5-3$ min. The transverse anisotropy of <5 keV electrons and the frequency-integrated intensity of whistler waves measured by THEMIS A and D show that intense whistlers were likely generated by anisotropic hot electrons that were also modulated by ULF waves over a wide (L, MLT) region. Low-altitude measurements of tens of keV precipitating electrons by ELFIN A and NOAA spacecraft confirm that intense equatorial whistlers were indeed present. Simultaneous observations at ground-based stations (KAN and LOZ) in good conjunction with the satellites demonstrate that such waves indeed propagated to the ground and, thus, show that these waves were ducted. Low-altitude measurements of precipitating and

trapped electron fluxes on ELFIN A CubeSat finally show that these ducted waves efficiently scattered relativistic electrons with energies up to $\sim$700 keV toward the loss cone.

2. In the second event in 2019-09-29 04:00-06:00 the near-equatorial ERG observed intense whistler-mode chorus waves in a wide L-shell range. Simultaneous observations of whistlers at ground-based stations (KAN and LOZ) demonstrate that such whistlers also propagated to the ground and, thus, were ducted waves. These observations are partly confirmed by low-altitude measurements of tens of keV precipitating electrons by ELFIN A and NOAA spacecraft, although both ELFIN A and NOAA orbits are well separated in MLT from ERG and ground-based stations. Low-altitude measurements of precipitating and trapped electron fluxes on ELFIN A CubeSat reveal that these ducted waves efficiently scattered relativistic electrons.
3. In the third and fourth events in 2019-10-06 00:00-02:00 and 2019-10-07 00:20-02:00, ERG observations either showed oblique waves (for $|\lambda| < 15^\circ$) or no waves (for $|\lambda| > 25^\circ$). NOAA spacecraft measurements of precipitating fluxes of >30 keV electrons indicate whistler-mode wave generation around the equator. These waves, however, were not seen on the conjugate ground-based station (LOZ). Thus, these equatorial whistler-mode waves were likely damped and did not reach middle latitudes, let alone the ionosphere. Low-altitude measurements of precipitating and trapped electron fluxes on ELFIN A show that these waves only scattered electrons with energies below 150 keV into the loss cone, in agreement with expectations based on the minimum resonant energy with those waves near the equator.

Although the obtained results are based on only four events, they suggest that whistler-mode wave ducting may play a significant role in losses of relativistic electrons, and that it may be important to include ducted whistlers into radiation belt models.

Acknowledgments

X.J.Z., A.V.A., and V.A. acknowledge support by NASA awards 80NSSC20K1270, NNX14AN68G, and NSF grants AGS-1242918, AGS-2019950, and AGS-2021749. A.G.D. and Y.V.F. acknowledge support by the Russian Ministry of Education and Science under state task AAAAA181180124901007. The work with KAN data was supported by the Academy of Finland under grants 330783 and 324025. We are grateful to NASAs CubeSat Launch Initiative for ELFIN's successful launch in the desired orbits. We acknowledge early support of ELFIN project by the AFOSR, under its University Nanosat Program, UNP-8 project, contract FA9453-12-D-0285, and by the California Space Grant program. We acknowledge critical contributions of numerous volunteer ELFIN team student members. ELFIN data is available at http://themis-data.igpp.ucla.edu/ela/, THEMIS data is avaliable at http://themis.ssl.berkeley.edu. Data access and processing was done using SPEDAS V3.1, see Angelopoulos et al. (2019). Data of ground-based VLF receivers is available at https://www.sgo.fi/pub_vlf/, http://aurora.pgia.ru/. Science data of the ERG (Arase) satellite were obtained from the ERG Science Center operated by ISAS/JAXA and ISEE/Nagoya University (https://ergsc.isee.nagoya-u.ac.jp/index.shtml.en, Miyoshi, Hori, et al. (2018)). The present study analyzed the HEP L2_v03_01 data (Mitani, Hori, et al., 2018), MEPe L2_v01_02 data (Y. Kasahara, Kojima, et al., 2018), MGF L2_v04_04 data (Matsuoka, Teramoto, Imajo, et al., 2018), PWE OFA L2_v02_01 data (S. Kasahara, Yokota, Hori, et al., 2018), and ORB L2_v03 data (Miyoshi, Shinohara, & Jun, 2018).

References

Agapitov, O. V., Artemyev, A., Krasnoselskikh, V., Khotyaintsev, Y. V., Mourenas, D., Breuillard, H., ... Rolland, G. (2013, June). Statistics of whistler mode waves in the outer radiation belt: Cluster STAFF-SA measurements. *J. Geophys. Res.*, *118*, 3407-3420. doi: 10.1002/jgra.50312

Agapitov, O. V., Artemyev, A. V., Mourenas, D., Mozer, F. S., & Krasnoselskikh, V. (2015, December). Empirical model of lower band chorus wave distribution in the outer radiation belt. *J. Geophys. Res.*, *120*, 10. doi: 10.1002/2015JA021829

Agapitov, O. V., Mourenas, D., Artemyev, A., Hospodarsky, G., & Bonnell, J. W. (2019, June). Time Scales for Electron Quasi-linear Diffusion by Lower-Band Chorus Waves: The Effects of wpe/wce Dependence on Geomagnetic Activity. *Geophys. Res. Lett.*, *46*, 6178-6187. doi: 10.1029/2019GL083446

Agapitov, O. V., Mourenas, D., Artemyev, A. V., Mozer, F. S., Hospodarsky, G., Bonnell, J., & Krasnoselskikh, V. (2018, January). Synthetic Empirical Chorus Wave Model From Combined Van Allen Probes and Cluster Statistics. *Journal of Geophysical Research (Space Physics)*, *123*(1), 297-314. doi: 10.1002/2017JA024843

Allison, H. J., & Shprits, Y. Y. (2020, September). Local heating of radiation belt electrons to ultra-relativistic energies. *Nature Communications*, *11*, 4533. doi: 10.1038/s41467-020-18053-z

Allison, H. J., Shprits, Y. Y., Zhelavskaya, I. S., Wang, D., & Smirnov, A. G. (2021, January). Gyroresonant wave-particle interactions with chorus waves during extreme depletions of plasma density in the Van Allen radiation belts. *Science Advances*, *7*(5), eabc0380. doi: 10.1126/sciadv.abc0380

Angelopoulos, V. (2008, December). The THEMIS Mission. *Space Sci. Rev.*, *141*, 5-34. doi: 10.1007/s11214-008-9336-1

Angelopoulos, V., Cruce, P., Drozdov, A., Grimes, E. W., Hatzigeorgiu, N., King, D. A., … Schroeder, P. (2019, January). The Space Physics Environment Data Analysis System (SPEDAS). *Space Sci. Rev.*, *215*, 9. doi: 10.1007/s11214-018-0576-4

Angelopoulos, V., Sibeck, D., Carlson, C. W., McFadden, J. P., Larson, D., Lin, R. P., … Sigwarth, J. (2008, December). First Results from the THEMIS Mission. *Space Sci. Rev.*, *141*, 453-476. doi: 10.1007/s11214-008-9378-4

Angelopoulos, V., Tsai, E., Bingley, L., Shaffer, C., Turner, D. L., Runov, A., … Zhang, G. Y. (2020, July). The ELFIN Mission. *Space Sci. Rev.*, *216*(5), 103. doi: 10.1007/s11214-020-00721-7

Artemyev, A. V., Agapitov, O., Mourenas, D., Krasnoselskikh, V., Shastun, V., & Mozer, F. (2016, April). Oblique Whistler-Mode Waves in the Earth's Inner Magnetosphere: Energy Distribution, Origins, and Role in Radiation Belt Dynamics. *Space Sci. Rev.*, *200*(1-4), 261-355. doi: 10.1007/s11214-016-0252-5

Artemyev, A. V., Agapitov, O. V., Mourenas, D., Krasnoselskikh, V. V., & Mozer, F. S. (2015, May). Wave energy budget analysis in the Earth's radiation belts uncovers a missing energy. *Nature Communications*, *6*, 8143. doi: 10.1038/ncomms8143

Artemyev, A. V., Zhang, X. J., Angelopoulos, V., Mourenas, D., Vainchtein, D., Shen, Y., … Runov, A. (2020, September). Ionosphere Feedback to Electron Scattering by Equatorial Whistler Mode Waves. *Journal of Geophysical Research (Space Physics)*, *125*(9), e28373. doi: 10.1029/2020JA028373

Auster, H. U., Glassmeier, K. H., Magnes, W., Aydogar, O., Baumjohann, W., Constantinescu, D., … Wiedemann, M. (2008, December). The THEMIS Fluxgate Magnetometer. *Space Sci. Rev.*, *141*, 235-264. doi: 10.1007/s11214-008-9365-9

Blum, L. W., Halford, A., Millan, R., Bonnell, J. W., Goldstein, J., Usanova, M., … Li, X. (2015, July). Observations of coincident EMIC wave activity and duskside energetic electron precipitation on 18-19 January 2013. *Geophys. Res. Lett.*, *42*, 5727-5735. doi: 10.1002/2015GL065245

Bortnik, J., Inan, U. S., & Bell, T. F. (2006, February). Landau damping and resultant unidirectional propagation of chorus waves. *Geophys. Res. Lett.*, *33*, 3102. doi: 10.1029/2005GL024553

Bortnik, J., Thorne, R. M., Meredith, N. P., & Santolik, O. (2007, August). Ray tracing of penetrating chorus and its implications for the radiation belts. *Geophys. Res. Lett.*, *34*, L15109. doi: 10.1029/2007GL030040

Breuillard, H., Zaliznyak, Y., Krasnoselskikh, V., Agapitov, O., Artemyev, A., &

Rolland, G. (2012). Chorus wave-normal statistics in the Earth's radiation belts from ray tracing technique. *Ann. Geophys.*, *30*, 1223-1233. doi: 10.5194/angeo-30-1223-2012
Chen, L., Breneman, A. W., Xia, Z., & Zhang, X.-j. (2020, September). Modeling of Bouncing Electron Microbursts Induced by Ducted Chorus Waves. *Geophys. Res. Lett.*, *47*(17), e89400. doi: 10.1029/2020GL089400
Chen, L., Thorne, R. M., Li, W., & Bortnik, J. (2013, March). Modeling the wave normal distribution of chorus waves. *J. Geophys. Res.*, *118*, 1074-1088. doi: 10.1029/2012JA018343
Chen, L., Zhang, X.-J., Artemyev, A., Zheng, L., Xia, Z., Breneman, A., & Horne, R. (2021). Electron microbursts induced by nonducted chorus waves. *Front. Phys.*. doi: 10.3389/fspas.2021.745927
Chen, R., Gao, X., Lu, Q., Chen, L., Tsurutani, B. T., Li, W., ... Wang, S. (2021, April). In Situ Observations of Whistler Mode Chorus Waves Guided by Density Ducts. *Journal of Geophysical Research (Space Physics)*, *126*(4), e28814. doi: 10.1029/2020JA028814
Chen, R., Gao, X., Lu, Q., Tsurutani, B. T., & Wang, S. (2021, March). Observational Evidence for Whistler Mode Waves Guided/Ducted by the Inner and Outer Edges of the Plasmapause. *Geophys. Res. Lett.*, *48*(6), e92652. doi: 10.1029/2021GL092652
Chen, Y., Reeves, G. D., & Friedel, R. H. W. (2007, September). The energization of relativistic electrons in the outer Van Allen radiation belt. *Nature Physics*, *3*, 614-617. doi: 10.1038/nphys655
Chu, X., Bortnik, J., Li, W., Ma, Q., Denton, R., Yue, C., ... Menietti, J. (2017, September). A neural network model of three-dimensional dynamic electron density in the inner magnetosphere. *Journal of Geophysical Research (Space Physics)*, *122*(9), 9183-9197. doi: 10.1002/2017JA024464
Cully, C. M., Bonnell, J. W., & Ergun, R. E. (2008, June). THEMIS observations of long-lived regions of large-amplitude whistler waves in the inner magnetosphere. *Geophys. Res. Lett.*, *35*, 17. doi: 10.1029/2008GL033643
Cully, C. M., Ergun, R. E., Stevens, K., Nammari, A., & Westfall, J. (2008, December). The THEMIS Digital Fields Board. *Space Sci. Rev.*, *141*, 343-355. doi: 10.1007/s11214-008-9417-1
Demekhov, A. G., Manninen, J., Santolík, O., & Titova, E. E. (2017, December). Conjugate Ground-Spacecraft Observations of VLF Chorus Elements. *Geophys. Res. Lett.*, *44*(23), 11,735-11,744. doi: 10.1002/2017GL076139
Demekhov, A. G., Titova, E. E., Maninnen, J., Pasmanik, D. L., Lubchich, A. A., Santolík, O., ... Turunen, T. (2020, May). Localization of the Source of Quasiperiodic VLF Emissions in the Magnetosphere by Using Simultaneous Ground and Space Observations: A Case Study. *Journal of Geophysical Research (Space Physics)*, *125*(5), e27776. doi: 10.1029/2020JA027776
Demekhov, A. G., Trakhtengerts, V. Y., Rycroft, M. J., & Nunn, D. (2006, December). Electron acceleration in the magnetosphere by whistler-mode waves of varying frequency. *Geomagnetism and Aeronomy*, *46*, 711-716. doi: 10.1134/S0016793206060053
Denton, R. E., Takahashi, K., Galkin, I. A., Nsumei, P. A., Huang, X., Reinisch, B. W., ... Hughes, W. J. (2006, April). Distribution of density along magnetospheric field lines. *J. Geophys. Res.*, *111*, 4213. doi: 10.1029/2005JA011414
Fedorenko, Y., Tereshchenko, E., Pilgaev, S., Grigoryev, V., & Blagoveshchenskaya, N. (2014, December). Polarization of ELF waves generated during "beat-wave" heating experiment near cutoff frequency of the Earth-ionosphere waveguide. *Radio Science*, *49*(12), 1254-1264. doi: 10.1002/2013RS005336
Fu, X., Cowee, M. M., Friedel, R. H., Funsten, H. O., Gary, S. P., Hospodarsky, G. B., ... Winske, D. (2014, October). Whistler anisotropy instabilities as the source of banded chorus: Van Allen Probes observations and particle-in-cell

simulations. *Journal of Geophysical Research (Space Physics)*, *119*, 8288-8298. doi: 10.1002/2014JA020364

Gao, X., Li, W., Bortnik, J., Thorne, R. M., Lu, Q., Ma, Q., ... Wang, S. (2015, June). The effect of different solar wind parameters upon significant relativistic electron flux dropouts in the magnetosphere. *J. Geophys. Res.*, *120*, 4324-4337. doi: 10.1002/2015JA021182

Ghaffari, R., Cully, C. M., Turner, D. L., & Reeves, G. D. (2020, November). Characteristics of Electron Precipitation During 40 Energetic Electron Injections Inferred via Subionospheric VLF Signal Propagation. *Journal of Geophysical Research (Space Physics)*, *125*(11), e27233. doi: 10.1029/2019JA027233

Goldstein, J., Pascuale, S., & Kurth, W. S. (2019, June). Epoch-Based Model for Stormtime Plasmapause Location. *Journal of Geophysical Research (Space Physics)*, *124*(6), 4462-4491. doi: 10.1029/2018JA025996

Grach, V. S., & Demekhov, A. G. (2020, February). Precipitation of Relativistic Electrons Under Resonant Interaction With Electromagnetic Ion Cyclotron Wave Packets. *Journal of Geophysical Research (Space Physics)*, *125*(2), e27358. doi: 10.1029/2019JA027358

Hanzelka, M., & Santolík, O. (2019, June). Effects of Ducting on Whistler Mode Chorus or Exohiss in the Outer Radiation Belt. *Geophys. Res. Lett.*, *46*(11), 5735-5745. doi: 10.1029/2019GL083115

Helliwell, R. A. (1965). *Whistlers and related ionospheric phenomena.* Stanford University Press, USA.

Hosseini, P., Agapitov, O., Harid, V., & Gołkowski, M. (2021, March). Evidence of Small Scale Plasma Irregularity Effects on Whistler Mode Chorus Propagation. *Geophys. Res. Lett.*, *48*(5), e92850. doi: 10.1029/2021GL092850

Inan, U. S., & Bell, T. F. (1977, July). The plasmapause as a VLF wave guide. *J. Geophys. Res.*, *82*, 2819-2827. doi: 10.1029/JA082i019p02819

Kanekal, S., & Miyoshi, Y. (2021, December). Dynamics of the terrestrial radiation belts: a review of recent results during the VarSITI (Variability of the Sun and Its Terrestrial Impact) era, 2014-2018. *Progress in Earth and Planetary Science*, *8*(1), 35. doi: 10.1186/s40645-021-00413-y

Karpman, V. I., & Kaufman, R. N. (1982, April). Whistler wave propagation in density ducts. *Journal of Plasma Physics*, *27*(2), 225-238. doi: 10.1017/S0022377800026556

Kasahara, S., Miyoshi, Y., Yokota, S., Kasahara, Y., Matsuda, S., Kumamoto, A., ... Shinohara, I. (2018). Pulsating aurora from electron scattering by chorus waves. *Nature*, *554*, 337-340. doi: 10.1038/nature25505

Kasahara, S., Yokota, S., Hori, T., Keika, K., Miyoshi, Y., & Shinohara, I. (2018). The mep-e instrument level-2 omni-directional flux data of exploration of energization and radiation in geospace (erg) arase satellite. *ERG Science Center, Institute for Space-Earth Environmental Research, Nagoya University*, *Version 01_02*. doi: 10.34515/DATA.ERG-02001

Kasahara, S., Yokota, S., Mitani, T., Asamura, K., Hirahara, M., Shibano, Y., & Takashima, T. (2018, May). Medium-energy particle experiments-electron analyzer (MEP-e) for the exploration of energization and radiation in geospace (ERG) mission. *Earth, Planets, and Space*, *70*(1), 69. doi: 10.1186/s40623-018-0847-z

Kasahara, Y., Kasaba, Y., Kojima, H., Yagitani, S., Ishisaka, K., Kumamoto, A., ... Shinohara, I. (2018, May). The Plasma Wave Experiment (PWE) on board the Arase (ERG) satellite. *Earth, Planets, and Space*, *70*(1), 86. doi: 10.1186/s40623-018-0842-4

Kasahara, Y., Kojima, H., Matsuda, S., Ozaki, S., M. Yagitani, Shoji, M., Nakamura, S., ... I., S. (2018). The pwe/ofa instrument level-2 power spectrum data of exploration of energization and radiation in geospace (erg) arase satellite. *ERG Science Center, Institute for Space-Earth Environmental Research,*

Nagoya, Version 01_02. doi: 10.34515/DATA.ERG-08000
Ke, Y., Chen, L., Gao, X., Lu, Q., Wang, X., Chen, R., ... Wang, S. (2021, April). Whistler Mode Waves Trapped by Density Irregularities in the Earth's Magnetosphere. *Geophys. Res. Lett.*, *48*(7), e92305. doi: 10.1029/2020GL092305
Kennel, C. F., & Petschek, H. E. (1966, January). Limit on Stably Trapped Particle Fluxes. *J. Geophys. Res.*, *71*, 1-28.
Kersten, T., Horne, R. B., Glauert, S. A., Meredith, N. P., Fraser, B. J., & Grew, R. S. (2014, November). Electron losses from the radiation belts caused by EMIC waves. *J. Geophys. Res.*, *119*, 8820-8837. doi: 10.1002/2014JA020366
Kimura, I. (1985, December). Whistler mode propagation in the earth and planetary magnetospheres and ray tracing techniques. *Space Sci. Rev.*, *42*, 449-466. doi: 10.1007/BF00214998
Laird, M. J., & Nunn, D. (1975, January). Full-wave VLF modes in a cylindrically symmetric enhancement of plasma density. *Planatary Space Science*, *23*(12), 1649-1657. doi: 10.1016/0032-0633(75)90092-6
Le Contel, O., Roux, A., Robert, P., Coillot, C., Bouabdellah, A., de La Porte, B., ... Larson, D. (2008, December). First Results of the THEMIS Search Coil Magnetometers. *Space Sci. Rev.*, *141*, 509-534. doi: 10.1007/s11214-008-9371-y
Li, W., Mourenas, D., Artemyev, A., Agapitov, O., Bortnik, J., Albert, J., ... Hospodarsky, G. B. (2014). Evidence of stronger pitch angle scattering loss caused by oblique whistler-mode waves as compared with quasi-parallel waves. *Geophys. Res. Lett.*, *41*, 6063-6070. doi: 10.1002/2014GL061260
Li, W., Ni, B., Thorne, R. M., Bortnik, J., Green, J. C., Kletzing, C. A., ... Hospodarsky, G. B. (2013, September). Constructing the global distribution of chorus wave intensity using measurements of electrons by the POES satellites and waves by the Van Allen Probes. *Geophys. Res. Lett.*, *40*, 4526-4532. doi: 10.1002/grl.50920
Li, W., Shen, X. C., Ma, Q., Capannolo, L., Shi, R., Redmon, R. J., ... Hospodarsky, G. B. (2019, Apr). Quantification of Energetic Electron Precipitation Driven by Plume Whistler Mode Waves, Plasmaspheric Hiss, and Exohiss. *Geophys. Res. Lett.*, *46*(7), 3615-3624. doi: 10.1029/2019GL082095
Li, W., Thorne, R. M., Bortnik, J., Baker, D. N., Reeves, G. D., Kanekal, S. G., ... Green, J. C. (2015, September). Solar wind conditions leading to efficient radiation belt electron acceleration: A superposed epoch analysis. *Geophys. Res. Lett.*, *42*, 6906-6915. doi: 10.1002/2015GL065342
Li, W., Thorne, R. M., Ma, Q., Ni, B., Bortnik, J., Baker, D. N., ... Claudepierre, S. G. (2014, June). Radiation belt electron acceleration by chorus waves during the 17 March 2013 storm. *J. Geophys. Res.*, *119*, 4681-4693. doi: 10.1002/2014JA019945
Lu, Q., Ke, Y., Wang, X., Liu, K., Gao, X., Chen, L., & Wang, S. (2019, Jun). Two-Dimensional gcPIC Simulation of Rising-Tone Chorus Waves in a Dipole Magnetic Field. *Journal of Geophysical Research (Space Physics)*, *124*(6), 4157-4167. doi: 10.1029/2019JA026586
Ma, Q., Li, W., Thorne, R. M., Ni, B., Kletzing, C. A., Kurth, W. S., ... Angelopoulos, V. (2015, February). Modeling inward diffusion and slow decay of energetic electrons in the Earth's outer radiation belt. *Geophys. Res. Lett.*, *42*, 987-995. doi: 10.1002/2014GL062977
Manninen, J., Kleimenova, N. G., Fedorenko, Y. V., Bespalov, P. A., & Turunen, T. (2014, September). New results of structured VLF emissions observed simultaneously at two closely located stations near L ~5.5. *Annales Geophysicae*, *32*(9), 1163-1167. doi: 10.5194/angeo-32-1163-2014
Manninen, J., Kleimenova, N. G., Kozyreva, O. V., Bespalov, P. A., & Kozlovsky, A. E. (2013, July). Non-typical ground-based quasi-periodic VLF emissions observed at $L\sum 5.3$ under quiet geomagnetic conditions at night.

Journal of Atmospheric and Solar-Terrestrial Physics, *99*, 123-128. doi: 10.1016/j.jastp.2012.05.007

Martinez-Calderon, C., Katoh, Y., Manninen, J., Kasahara, Y., Matsuda, S., Kumamoto, A., ... Miyoshi, Y. (2020, January). Conjugate Observations of Dayside and Nightside VLF Chorus and QP Emissions Between Arase (ERG) and Kannuslehto, Finland. *Journal of Geophysical Research (Space Physics)*, *125*(1), e26663. doi: 10.1029/2019JA026663

Martinez-Calderon, C., Shiokawa, K., Miyoshi, Y., Keika, K., Ozaki, M., Schofield, I., ... Kurth, W. S. (2016, June). ELF/VLF wave propagation at subauroral latitudes: Conjugate observation between the ground and Van Allen Probes A. *Journal of Geophysical Research (Space Physics)*, *121*(6), 5384-5393. doi: 10.1002/2015JA022264

Martinez-Calderon, C., Shiokawa, K., Miyoshi, Y., Ozaki, M., Schofield, I., & Connors, M. (2015, October). Statistical study of ELF/VLF emissions at subauroral latitudes in Athabasca, Canada. *Journal of Geophysical Research (Space Physics)*, *120*(10), 8455-8469. doi: 10.1002/2015JA021347

Matsuda, S., Kasahara, Y., Kojima, H., Kasaba, Y., Yagitani, S., Ozaki, M., ... Shinohara, I. (2018, May). Onboard software of Plasma Wave Experiment aboard Arase: instrument management and signal processing of Waveform Capture/Onboard Frequency Analyzer. *Earth, Planets, and Space*, *70*(1), 75. doi: 10.1186/s40623-018-0838-0

Matsuoka, A., Teramoto, M., Imajo, S., Kurita, S., Miyoshi, Y., & Shinohara, I. (2018). The mgf instrument level-2 high-resolution magnetic field data of exploration of energization and radiation in geospace (erg) arase satellite. *ERG Science Center, Institute for Space-Earth Environmental Research, Nagoya*, *Version 04_04*. doi: 10.34515/DATA.ERG-06000

Matsuoka, A., Teramoto, M., Nomura, R., Nosé, M., Fujimoto, A., Tanaka, Y., ... Shinohara, I. (2018, March). The ARASE (ERG) magnetic field investigation. *Earth, Planets, and Space*, *70*(1), 43. doi: 10.1186/s40623-018-0800-1

Maxworth, A. S., & Golkowski, M. (2017). Magnetospheric whistler mode ray tracing in a warm background plasma with finite electron and ion temperature. *J. Geophys. Res.*, *122*(7), 7323–7335. Retrieved from `http://dx.doi.org/10.1002/2016JA023546` doi: 10.1002/2016JA023546

McFadden, J. P., Carlson, C. W., Larson, D., Ludlam, M., Abiad, R., Elliott, B., ... Angelopoulos, V. (2008, December). The THEMIS ESA Plasma Instrument and In-flight Calibration. *Space Sci. Rev.*, *141*, 277-302. doi: 10.1007/s11214-008-9440-2

Meredith, N. P., Horne, R. B., & Anderson, R. R. (2001, July). Substorm dependence of chorus amplitudes: Implications for the acceleration of electrons to relativistic energies. *J. Geophys. Res.*, *106*, 13165-13178. doi: 10.1029/2000JA900156

Meredith, N. P., Horne, R. B., Sicard-Piet, A., Boscher, D., Yearby, K. H., Li, W., & Thorne, R. M. (2012, October). Global model of lower band and upper band chorus from multiple satellite observations. *J. Geophys. Res.*, *117*, 10225. doi: 10.1029/2012JA017978

Meredith, N. P., Horne, R. B., Thorne, R. M., & Anderson, R. R. (2003, August). Favored regions for chorus-driven electron acceleration to relativistic energies in the Earth's outer radiation belt. *Geophys. Res. Lett.*, *30*(16), 160000-1. doi: 10.1029/2003GL017698

Millan, R. M., & Baker, D. N. (2012, November). Acceleration of Particles to High Energies in Earth's Radiation Belts. *Space Sci. Rev.*, *173*, 103-131. doi: 10.1007/s11214-012-9941-x

Millan, R. M., & Thorne, R. M. (2007, March). Review of radiation belt relativistic electron losses. *Journal of Atmospheric and Solar-Terrestrial Physics*, *69*, 362-377. doi: 10.1016/j.jastp.2006.06.019

Mitani, T., Hori, T., Park, I., Takashima, T., Miyoshi, Y., & Shinohara, I. (2018). The hep instrument level-2 omni-directional flux data of exploration of energization and radiation in geospace (erg) arase satellite. *ERG Science Center, Institute for Space-Earth Environmental Research, Nagoya*, *Version 03_01*. doi: 10.34515/DATA.ERG-01001

Mitani, T., Takashima, T., Kasahara, S., Miyake, W., & Hirahara, M. (2018, May). High-energy electron experiments (HEP) aboard the ERG (Arase) satellite. *Earth, Planets, and Space*, *70*(1), 77. doi: 10.1186/s40623-018-0853-1

Miyoshi, Y., Hori, T., Shoji, M., Teramoto, M., Chang, T. F., Segawa, T., . . . Shinohara, I. (2018, June). The ERG Science Center. *Earth, Planets, and Space*, *70*(1), 96. doi: 10.1186/s40623-018-0867-8

Miyoshi, Y., Hosokawa, S., Kurita, S.-I., Oyama, Y., Ogawa, S., Saito, I., . . . Nakamura (2021). Penetration of MeV electrons into the mesosphere accompanying pulsating aurorae. *Scientific Reports*, *11*, 13724. doi: 10.1038/s41598-021-92611-3

Miyoshi, Y., Morioka, A., Misawa, H., Obara, T., Nagai, T., & Kasahara, Y. (2003, January). Rebuilding process of the outer radiation belt during the 3 November 1993 magnetic storm: NOAA and Exos-D observations. *J. Geophys. Res.*, *108*, 1004. doi: 10.1029/2001JA007542

Miyoshi, Y., Saito, S., Kurita, S., Asamura, K., Hosokawa, K., Sakanoi, T., . . . Blake, J. B. (2020, November). Relativistic Electron Microbursts as High-Energy Tail of Pulsating Aurora Electrons. *Geophys. Res. Lett.*, *47*(21), e90360. doi: 10.1029/2020GL090360

Miyoshi, Y., Saito, S., Seki, K., Nishiyama, T., Kataoka, R., Asamura, K., . . . Santolik, O. (2015, September). Relation between fine structure of energy spectra for pulsating aurora electrons and frequency spectra of whistler mode chorus waves. *J. Geophys. Res.*, *120*, 7728-7736. doi: 10.1002/2015JA021562

Miyoshi, Y., Shinohara, I., & Jun, C.-W. (2018). The level-2 orbit data of exploration of energization and radiation in geospace (erg) arase satellite. *ERG Science Center, Institute for Space-Earth Environmental Research, Nagoya*, *Version v03*. doi: 10.34515/DATA.ERG-12000

Miyoshi, Y., Shinohara, I., Takashima, T., Asamura, K., Higashio, N., Mitani, T., . . . Seki, K. (2018, June). Geospace exploration project ERG. *Earth, Planets, and Space*, *70*(1), 101. doi: 10.1186/s40623-018-0862-0

Motoba, T., Takahashi, K., Gjerloev, J., Ohtani, S., & Milling, D. K. (2013, December). The role of compressional Pc5 pulsations in modulating precipitation of energetic electrons. *Journal of Geophysical Research (Space Physics)*, *118*(12), 7728-7739. doi: 10.1002/2013JA018912

Mourenas, D., Artemyev, A. V., Agapitov, O. V., & Krasnoselskikh, V. (2014, April). Consequences of geomagnetic activity on energization and loss of radiation belt electrons by oblique chorus waves. *J. Geophys. Res.*, *119*, 2775-2796. doi: 10.1002/2013JA019674

Mourenas, D., Artemyev, A. V., Agapitov, O. V., Krasnoselskikh, V., & Li, W. (2014, December). Approximate analytical solutions for the trapped electron distribution due to quasi-linear diffusion by whistler mode waves. *J. Geophys. Res.*, *119*, 9962-9977. doi: 10.1002/2014JA020443

Mourenas, D., Artemyev, A. V., Ma, Q., Agapitov, O. V., & Li, W. (2016, May). Fast dropouts of multi-MeV electrons due to combined effects of EMIC and whistler mode waves. *Geophys. Res. Lett.*, *43*(9), 4155-4163. doi: 10.1002/2016GL068921

Namekawa, T., Mitani, T., Asamura, K., Miyoshi, Y., Hosokawa, K., Ogawa, Y., . . . Koehler, C. (2021). Rocket observation of sub-relativistic electrons in the quiet dayside auroral ionosphere. *Journal of Geophysical Research: Space Physics*, *126*(7), e2020JA028633. doi: https://doi.org/10.1029/2020JA028633

Ni, B., Li, W., Thorne, R. M., Bortnik, J., Green, J. C., Kletzing, C. A., . . . Soria-

Santacruz Pich, M. (2014, July). A novel technique to construct the global distribution of whistler mode chorus wave intensity using low-altitude POES electron data. *J. Geophys. Res.*, *119*, 5685-5699. doi: 10.1002/2014JA019935

Nishimura, Y., Bortnik, J., Li, W., Thorne, R. M., Lyons, L. R., Angelopoulos, V., ... Auster, U. (2010, October). Identifying the Driver of Pulsating Aurora. *Science*, *330*, 81-84. doi: 10.1126/science.1193186

O'Brien, T. P., & Moldwin, M. B. (2003, February). Empirical plasmapause models from magnetic indices. *Geophys. Res. Lett.*, *30*, 1152. doi: 10.1029/2002GL016007

Pasmanik, D. L., & Trakhtengerts, V. Y. (2005, June). Dispersion properties of ducted whistlers, generated by lightning discharge. *Annales Geophysicae*, *23*(4), 1433-1439. doi: 10.5194/angeo-23-1433-2005

Santolík, O., Macúšová, E., Kolmašová, I., Cornilleau-Wehrlin, N., & Conchy, Y. (2014, April). Propagation of lower-band whistler-mode waves in the outer Van Allen belt: Systematic analysis of 11 years of multi-component data from the Cluster spacecraft. *Geophys. Res. Lett.*, *41*, 2729-2737. doi: 10.1002/2014GL059815

Sheeley, B. W., Moldwin, M. B., Rassoul, H. K., & Anderson, R. R. (2001, November). An empirical plasmasphere and trough density model: CRRES observations. *J. Geophys. Res.*, *106*, 25631-25642. doi: 10.1029/2000JA000286

Shiokawa, K., Katoh, Y., Hamaguchi, Y., Yamamoto, Y., Adachi, T., Ozaki, M., ... Karjala, M. (2017, November). Ground-based instruments of the PWING project to investigate dynamics of the inner magnetosphere at subauroral latitudes as a part of the ERG-ground coordinated observation network. *Earth, Planets, and Space*, *69*(1), 160. doi: 10.1186/s40623-017-0745-9

Shiokawa, K., Yokoyama, Y., Ieda, A., Miyoshi, Y., Nomura, R., Lee, S., ... Connors, M. (2014, September). Ground-based ELF/VLF chorus observations at subauroral latitudes – VLF-CHAIN Campaign. *Journal of Geophysical Research (Space Physics)*, *119*(9), 7363-7379. doi: 10.1002/2014JA020161

Shklyar, D. R., Chum, J., & Jirícek, F. (2004, October). Characteristic properties of Nu whistlers as inferred from observations and numerical modelling. *Annales Geophysicae*, *22*, 3589-3606. doi: 10.5194/angeo-22-3589-2004

Shprits, Y. Y., Drozdov, A. Y., Spasojevic, M., Kellerman, A. C., Usanova, M. E., Engebretson, M. J., ... Aseev, N. A. (2016, September). Wave-induced loss of ultra-relativistic electrons in the Van Allen radiation belts. *Nature Communications*, *7*, 12883. doi: 10.1038/ncomms12883

Shprits, Y. Y., Subbotin, D. A., Meredith, N. P., & Elkington, S. R. (2008, November). Review of modeling of losses and sources of relativistic electrons in the outer radiation belt II: Local acceleration and loss. *Journal of Atmospheric and Solar-Terrestrial Physics*, *70*, 1694-1713. doi: 10.1016/j.jastp.2008.06.014

Shprits, Y. Y., Thorne, R. M., Horne, R. B., & Summers, D. (2006, October). Bounce-averaged diffusion coefficients for field-aligned chorus waves. *J. Geophys. Res.*, *111*, 10225. doi: 10.1029/2006JA011725

Sorathia, K. A., Merkin, V. G., Ukhorskiy, A. Y., Mauk, B. H., & Sibeck, D. G. (2017, September). Energetic particle loss through the magnetopause: A combined global MHD and test-particle study. *Journal of Geophysical Research (Space Physics)*, *122*(9), 9329-9343. doi: 10.1002/2017JA024268

Spasojevic, M. (2014, October). Statistical analysis of ground-based chorus observations during geomagnetic storms. *Journal of Geophysical Research (Space Physics)*, *119*(10), 8299-8317. doi: 10.1002/2014JA019975

Streltsov, A. V., & Bengtson, M. T. (2020, October). Observations and Modeling of Whistler Mode Waves in the Magnetospheric Density Ducts. *Journal of Geophysical Research (Space Physics)*, *125*(10), e28398. doi: 10.1029/2020JA028398

Summers, D., & Ni, B. (2008, July). Effects of latitudinal distributions of particle density and wave power on cyclotron resonant diffusion rates of radiation belt electrons. *Earth, Planets, and Space*, *60*, 763-771.

Summers, D., Ni, B., & Meredith, N. P. (2007, April). Timescales for radiation belt electron acceleration and loss due to resonant wave-particle interactions: 2. Evaluation for VLF chorus, ELF hiss, and electromagnetic ion cyclotron waves. *J. Geophys. Res.*, *112*, 4207. doi: 10.1029/2006JA011993

Summers, D., & Thorne, R. M. (2003, April). Relativistic electron pitch-angle scattering by electromagnetic ion cyclotron waves during geomagnetic storms. *J. Geophys. Res.*, *108*, 1143. doi: 10.1029/2002JA009489

Summers, D., Thorne, R. M., & Xiao, F. (1998, September). Relativistic theory of wave-particle resonant diffusion with application to electron acceleration in the magnetosphere. *J. Geophys. Res.*, *103*, 20487-20500. doi: 10.1029/98JA01740

Tao, X., & Bortnik, J. (2010, October). Nonlinear interactions between relativistic radiation belt electrons and oblique whistler mode waves. *Nonlinear Processes in Geophysics*, *17*, 599-604. doi: 10.5194/npg-17-599-2010

Tao, X., Lu, Q., Wang, S., & Dai, L. (2014, October). Effects of magnetic field configuration on the day-night asymmetry of chorus occurrence rate: A numerical study. *Geophys. Res. Lett.*, *41*, 6577-6582. doi: 10.1002/2014GL061493

Thorne, R. M. (2010, November). Radiation belt dynamics: The importance of wave-particle interactions. *Geophys. Res. Lett.*, *372*, 22107. doi: 10.1029/2010GL044990

Thorne, R. M., & Kennel, C. F. (1971). Relativistic electron precipitation during magnetic storm main phase. *J. Geophys. Res.*, *76*, 4446. doi: 10.1029/JA076i019p04446

Thorne, R. M., Li, W., Ni, B., Ma, Q., Bortnik, J., Chen, L., ... Kanekal, S. G. (2013, December). Rapid local acceleration of relativistic radiation-belt electrons by magnetospheric chorus. *Nature*, *504*, 411-414. doi: 10.1038/nature12889

Thorne, R. M., O'Brien, T. P., Shprits, Y. Y., Summers, D., & Horne, R. B. (2005, September). Timescale for MeV electron microburst loss during geomagnetic storms. *J. Geophys. Res.*, *110*, 9202. doi: 10.1029/2004JA010882

Titova, E. E., Demekhov, A. G., Manninen, J., Pasmanik, D. L., & Larchenko, A. V. (2017, November). Localization of the sources of narrow-band noise VLF emissions in the range 4-10 kHz from simultaneous ground-based and Van Allen Probes satellite observations. *Geomagnetism and Aeronomy*, *57*(6), 706-718. doi: 10.1134/S0016793217060135

Titova, E. E., Kozelov, B. V., Demekhov, A. G., Manninen, J., Santolik, O., Kletzing, C. A., & Reeves, G. (2015). Identification of the source of quasi-periodic VLF emissions using ground-based and Van Allen Probes satellite observations. *Geophys. Res. Lett.*. doi: 10.1002/2015GL064911

Trakhtengerts, V. Y. (1963). The Mechanism of Generation of Very Low Frequency Electromagnetic Radiation in the Earth's Outer Radiation Belt. *Geomagnetism and Aeronomy*, *3*, 365.

Tsurutani, B. T., & Smith, E. J. (1974, January). Postmidnight chorus: A substorm phenomenon. *J. Geophys. Res.*, *79*, 118-127. doi: 10.1029/JA079i001p00118

Tsyganenko, N. A. (1995, April). Modeling the Earth's magnetospheric magnetic field confined within a realistic magnetopause. *J. Geophys. Res.*, *100*, 5599-5612. doi: 10.1029/94JA03193

Turner, D. L., Shprits, Y., Hartinger, M., & Angelopoulos, V. (2012, March). Explaining sudden losses of outer radiation belt electrons during geomagnetic storms. *Nature Physics*, *8*, 208-212. doi: 10.1038/nphys2185

Usanova, M. E., Drozdov, A., Orlova, K., Mann, I. R., Shprits, Y., Robertson, M. T., ... Wygant, J. (2014, March). Effect of EMIC waves on relativistic and ultrarelativistic electron populations: Ground-based and Van Allen Probes ob-

servations. *Geophys. Res. Lett.*, *41*, 1375-1381. doi: 10.1002/2013GL059024
Wang, D., & Shprits, Y. Y. (2019, July). On How High-Latitude Chorus Waves Tip the Balance Between Acceleration and Loss of Relativistic Electrons. *Geophys. Res. Lett.*, *46*(14), 7945-7954. doi: 10.1029/2019GL082681
Wang, D., Shprits, Y. Y., Zhelavskaya, I. S., Agapitov, O. V., Drozdov, A. Y., & Aseev, N. A. (2019, Feb). Analytical Chorus Wave Model Derived from Van Allen Probe Observations. *Journal of Geophysical Research (Space Physics)*, *124*(2), 1063-1084. doi: 10.1029/2018JA026183
Watt, C. E. J., Degeling, A. W., & Rankin, R. (2013, May). Constructing the frequency and wave normal distribution of whistler-mode wave power. *J. Geophys. Res.*, *118*, 1984-1991. doi: 10.1002/jgra.50231
Woodroffe, J. R., Jordanova, V. K., Funsten, H. O., Streltsov, A. V., Bengtson, M. T., Kletzing, C. A., ... Breneman, A. W. (2017, March). Van Allen Probes observations of structured whistler mode activity and coincident electron Landau acceleration inside a remnant plasmaspheric plume. *Journal of Geophysical Research (Space Physics)*, *122*(3), 3073-3086. doi: 10.1002/2015JA022219
Woodroffe, J. R., & Streltsov, A. V. (2013, February). Whistler propagation in the plasmapause. *Journal of Geophysical Research (Space Physics)*, *118*(2), 716-723. doi: 10.1002/jgra.50135
Yamaguchi, K., Matsumuro, T., Omura, Y., & Nunn, D. (2013, April). Ray tracing of whistler-mode chorus elements: implications for generation mechanisms of rising and falling tone emissions. *Annales Geophysicae*, *31*, 665-673. doi: 10.5194/angeo-31-665-2013
Zhang, X. J., Angelopoulos, V., Artemyev, A. V., Hartinger, M. D., & Bortnik, J. (2020, October). Modulation of Whistler Waves by Ultra-Low-Frequency Perturbations: The Importance of Magnetopause Location. *Journal of Geophysical Research (Space Physics)*, *125*(10), e28334. doi: 10.1029/2020JA028334
Zhang, X.-J., Chen, L., Artemyev, A. V., Angelopoulos, V., & Liu, X. (2019, November). Periodic Excitation of Chorus and ECH Waves Modulated by Ultralow Frequency Compressions. *Journal of Geophysical Research (Space Physics)*, *124*(11), 8535-8550. doi: 10.1029/2019JA027201
Zhang, X. J., Mourenas, D., Artemyev, A. V., Angelopoulos, V., Bortnik, J., Thorne, R. M., ... Hospodarsky, G. B. (2019, July). Nonlinear Electron Interaction With Intense Chorus Waves: Statistics of Occurrence Rates. *Geophys. Res. Lett.*, *46*(13), 7182-7190. doi: 10.1029/2019GL083833
Zhang, X. J., Mourenas, D., Shen, X. C., Qin, M., Artemyev, A. V., Ma, Q., ... Angelopoulos, V. (2021, May). Dependence of Relativistic Electron Precipitation in the Ionosphere on EMIC Wave Minimum Resonant Energy at the Conjugate Equator. *Journal of Geophysical Research (Space Physics)*, *126*(5), e29193. doi: 10.1029/2021JA029193
Zhelavskaya, I. S., Shprits, Y. Y., & Spasojević, M. (2017, November). Empirical Modeling of the Plasmasphere Dynamics Using Neural Networks. *Journal of Geophysical Research (Space Physics)*, *122*(11), 11,227-11,244. doi: 10.1002/2017JA024406

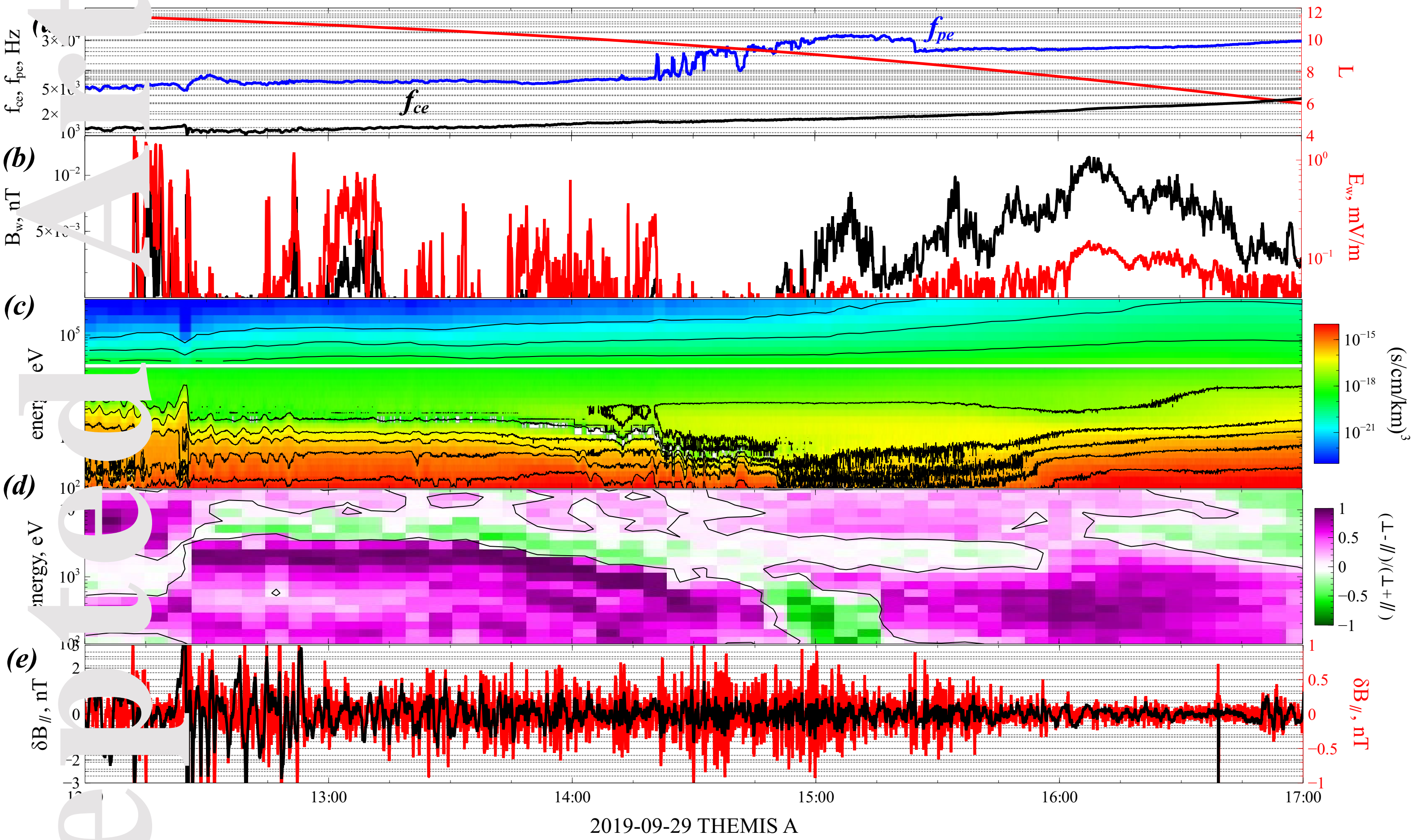

This article has been accepted for publication and undergone full peer review but has not been through the copyediting, typesetting, pagination and proofreading process, which may lead to differences between this version and the Version of Record. Please cite this article as doi: 10.1029/2021JA029851.

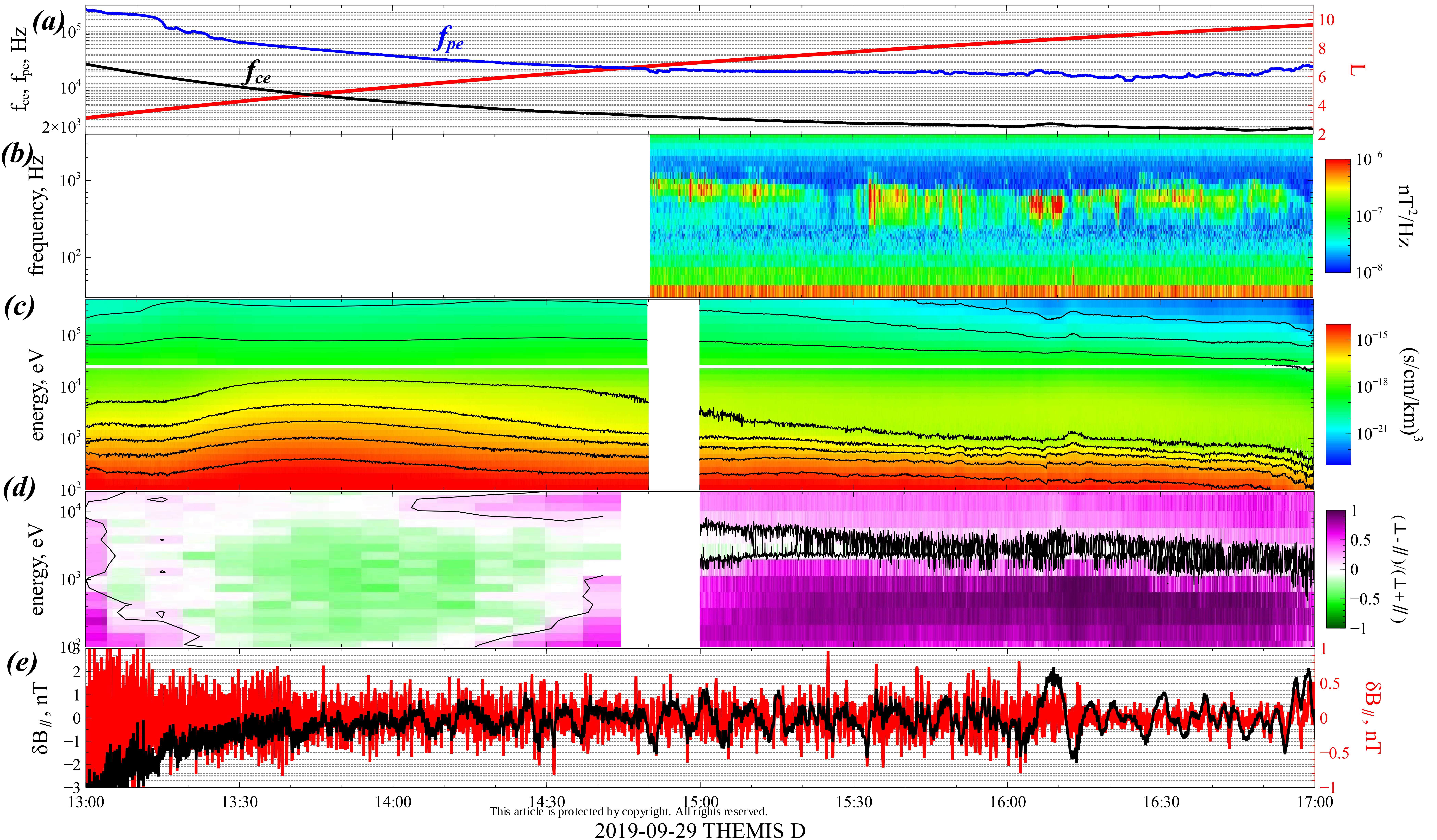

(a)
(b)
(c)
(d)
(e)
f_{pe}
f_{ce}
f_{ce}, f_{pe}, Hz
L
frequency, Hz
nT²/Hz
energy, eV
(s/cm/km)³
(//−⊥)/(//+⊥)
δB//, nT
13:00
13:30
14:00
14:30
15:00
15:30
16:00
16:30
17:00
2019-09-29 THEMIS D

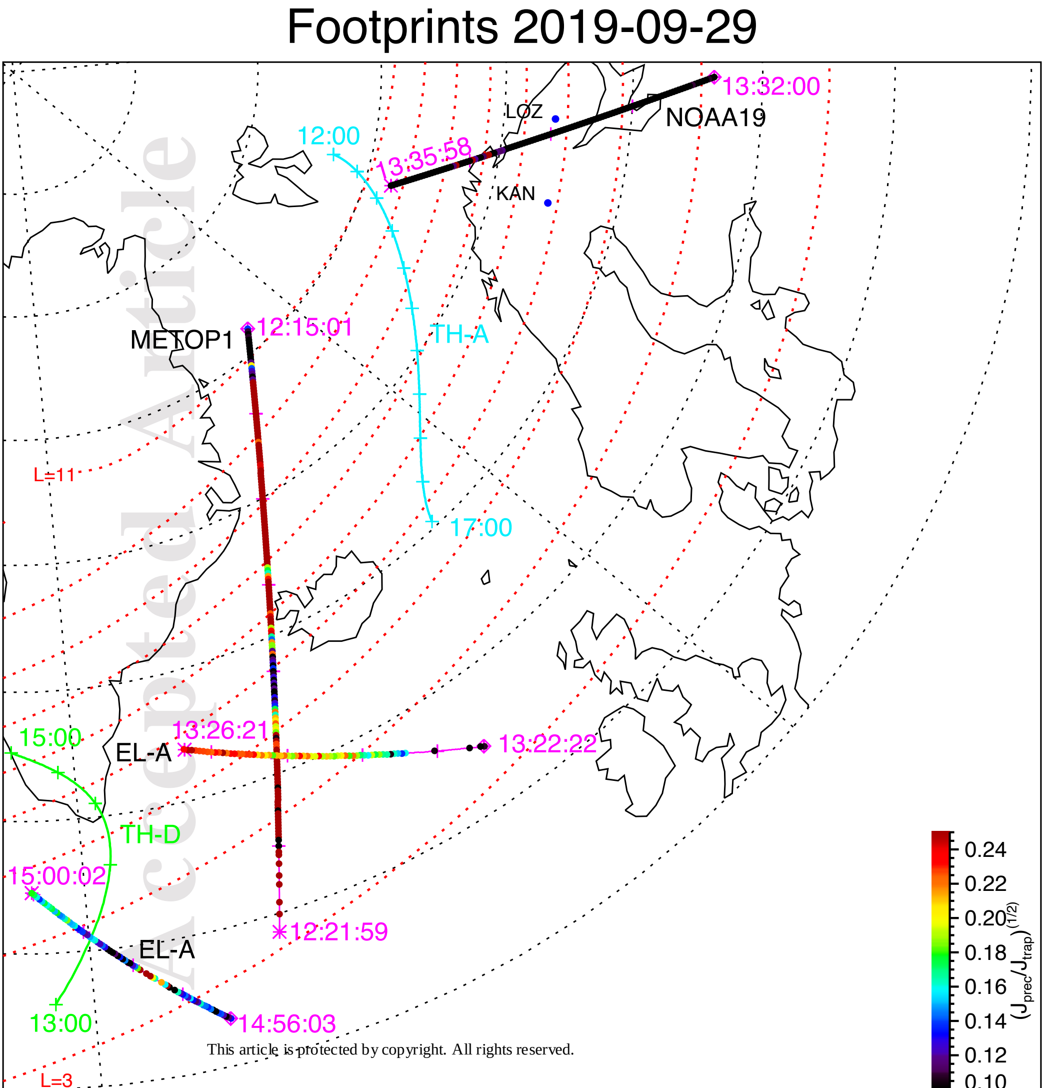
Footprints 2019-09-29
13:32:00
LOZ
NOAA19
12:00
13:35:58
KAN
12:15:01
METOP1
TH-A
L=11
17:00
13:26:21
13:22:22
15:00
EL-A
TH-D
15:00:02
EL-A
13:00
14:56:03
L=3
12:21:59
0.24
0.22
0.20
0.18
0.16
0.14
0.12
0.10
$(J_{prec}/J_{trap})^{(1/2)}$

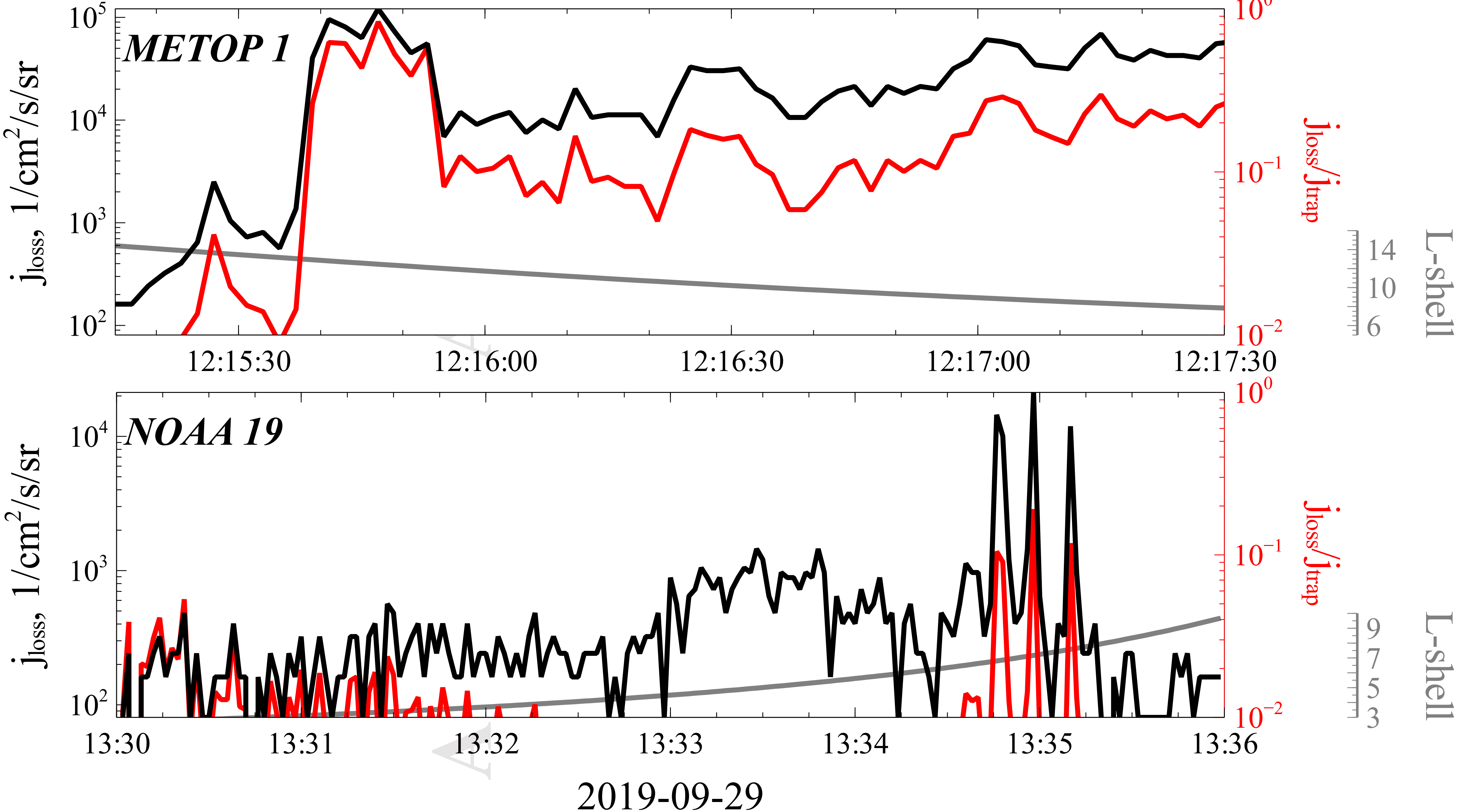
METOP 1
j_{loss}, 1/cm^2/s/sr
j_{loss}/j_{trap}
L-shell
12:15:30
12:16:00
12:16:30
12:17:00
12:17:30
NOAA 19
13:30
13:31
13:32
13:33
13:34
13:35
13:36
2019-09-29

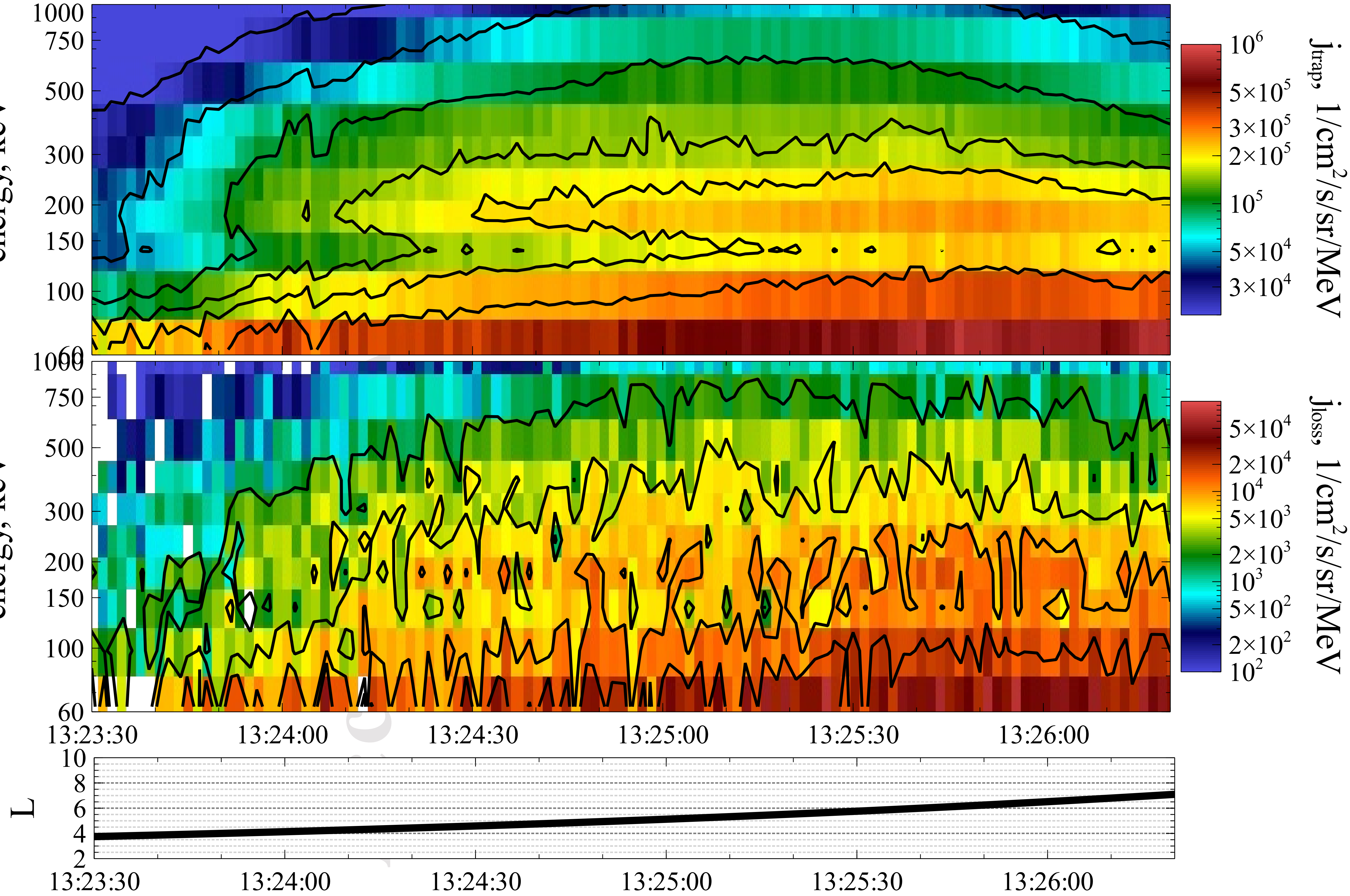

2019-09-29, ELFIN A

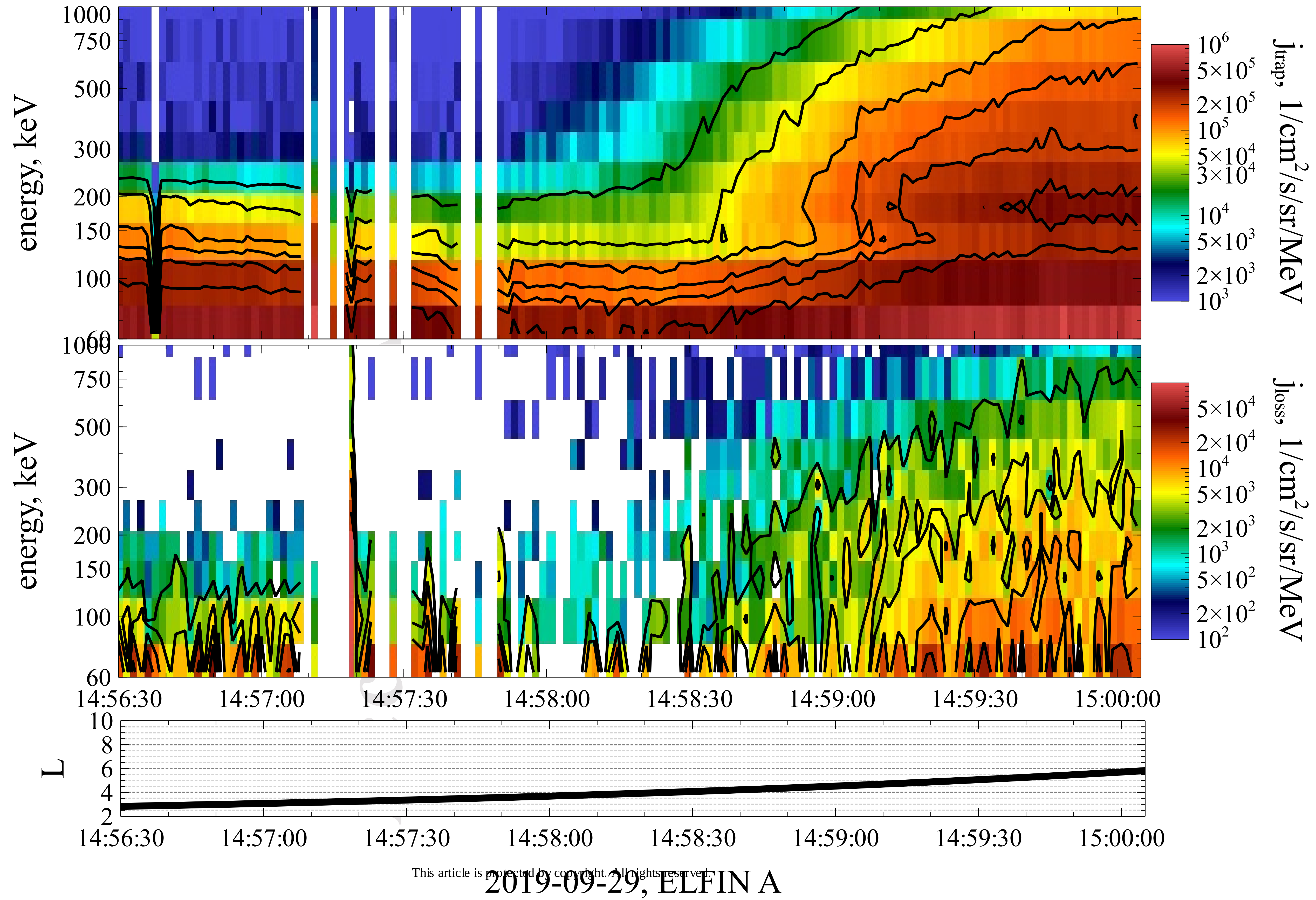
energy, keV
1000
750
500
300
200
150
100
60
j_{trap}, 1/cm^2/s/sr/MeV
10^6
5×10^5
2×10^5
10^5
5×10^4
3×10^4
10^4
5×10^3
2×10^3
10^3
j_{loss}, 1/cm^2/s/sr/MeV
5×10^4
2×10^4
10^4
5×10^3
2×10^3
10^3
5×10^2
2×10^2
10^2
14:56:30
14:57:00
14:57:30
14:58:00
14:58:30
14:59:00
14:59:30
15:00:00
L
10
8
6
4
2
2019-09-29, ELFIN A

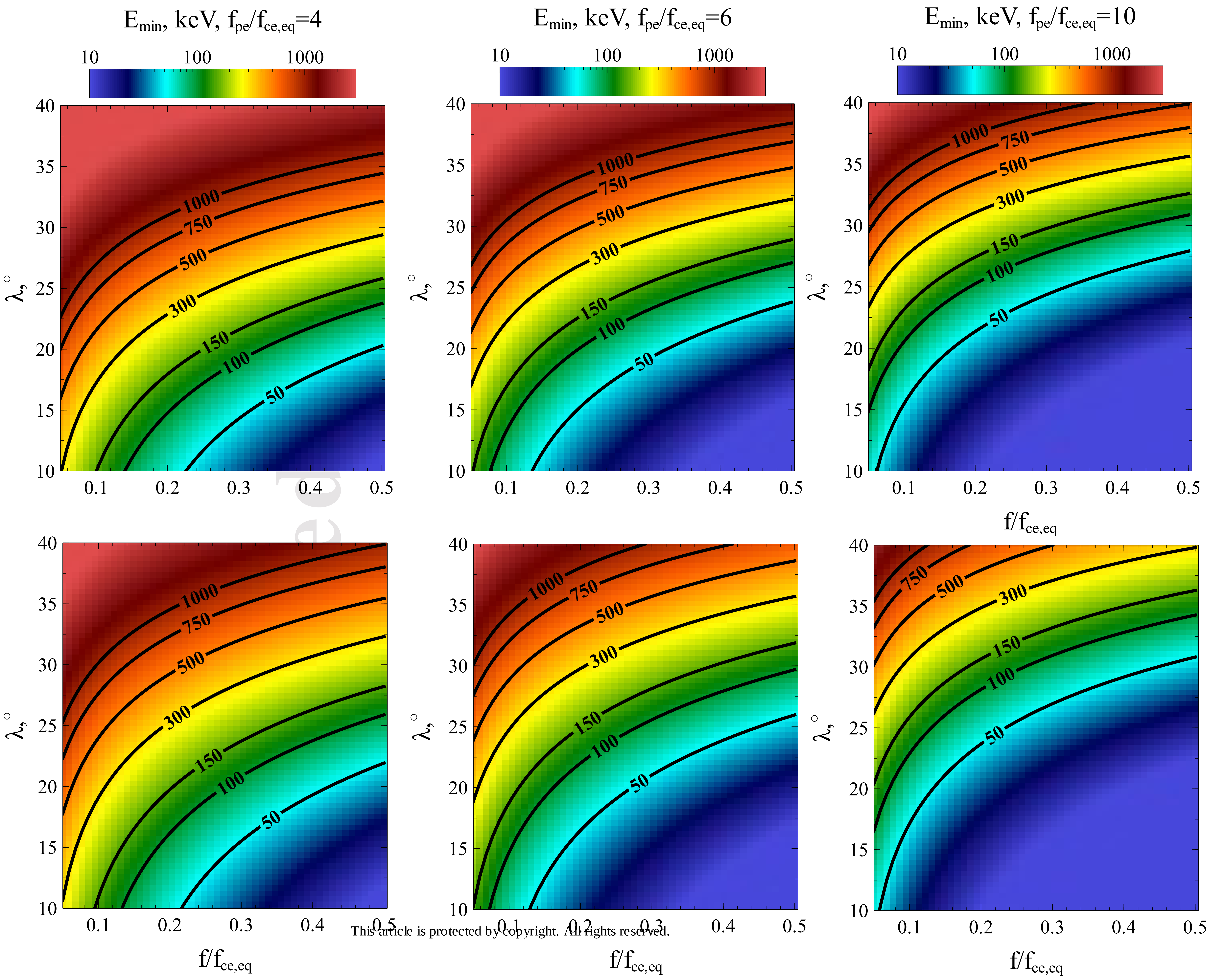

E_{min}, keV, $f_{pe}/f_{ce,eq}$=4
E_{min}, keV, $f_{pe}/f_{ce,eq}$=6
E_{min}, keV, $f_{pe}/f_{ce,eq}$=10
10
100
1000
λ,°
$f/f_{ce,eq}$
1000
750
500
300
150
100
50

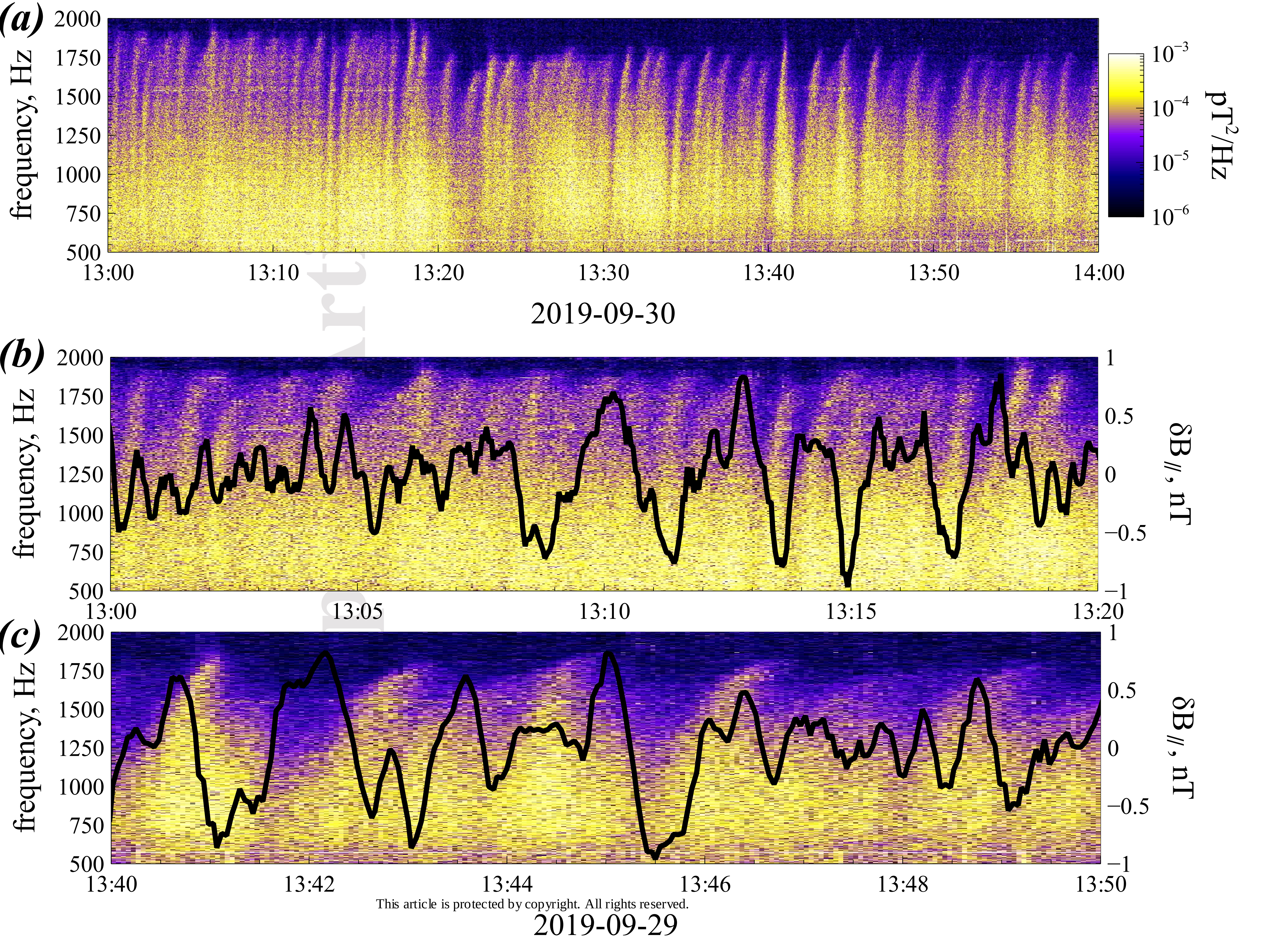

(a)
frequency, Hz
2000
1750
1500
1250
1000
750
500
13:00
13:10
13:20
13:30
13:40
13:50
14:00
2019-09-30
10^{-3}
10^{-4}
10^{-5}
10^{-6}
pT^2/Hz
(b)
13:00
13:05
13:10
13:15
13:20
1
0.5
0
−0.5
−1
δB$_{//}$, nT
(c)
13:40
13:42
13:44
13:46
13:48
13:50
2019-09-29

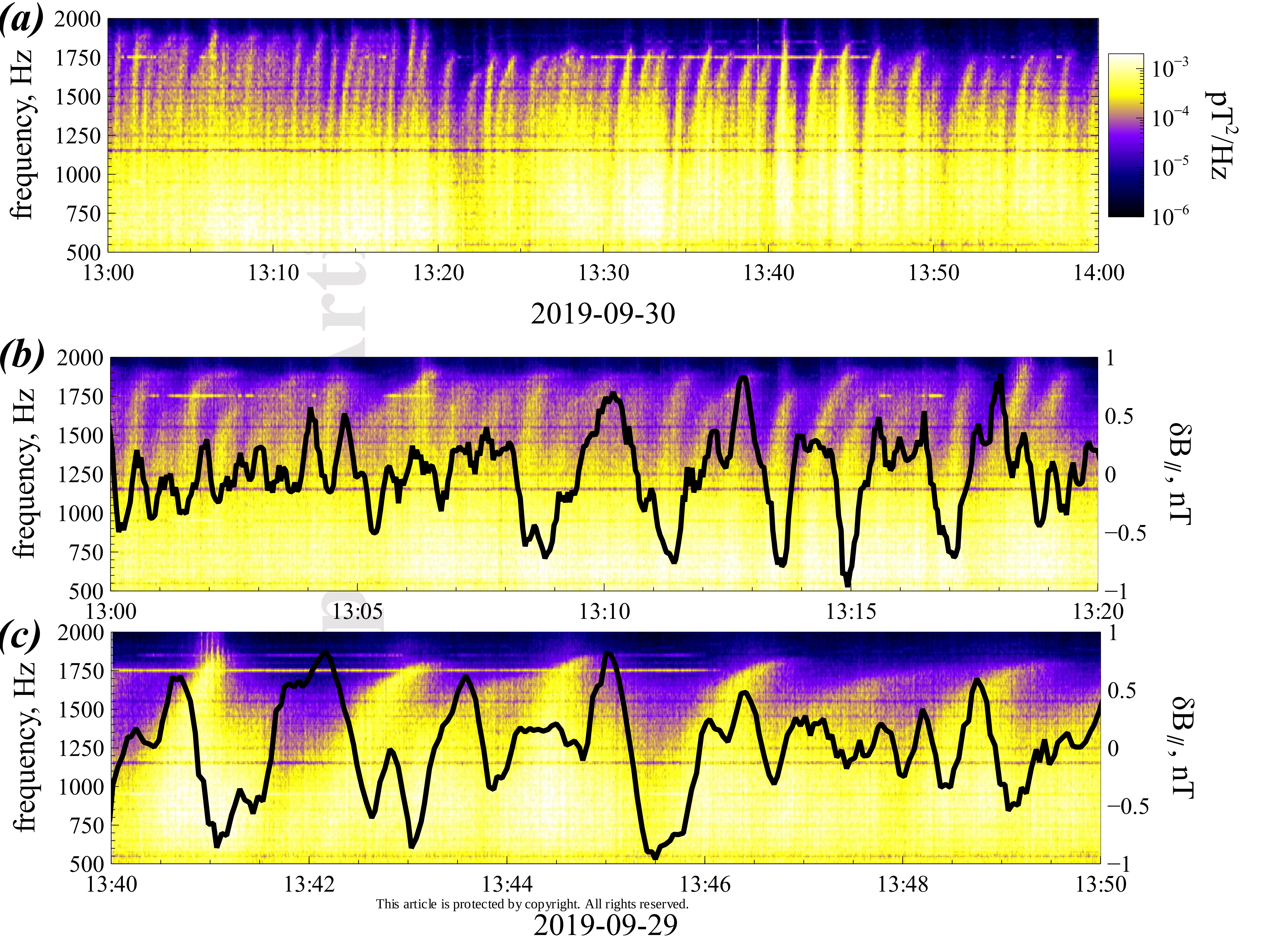

(a)
frequency, Hz
2000
1750
1500
1250
1000
750
500
13:00
13:10
13:20
13:30
13:40
13:50
14:00
2019-09-30
pT^2/Hz
10^{-3}
10^{-4}
10^{-5}
10^{-6}
(b)
13:00
13:05
13:10
13:15
13:20
δB$_{//}$, nT
1
0.5
0
−0.5
−1
(c)
13:40
13:42
13:44
13:46
13:48
13:50
2019-09-29

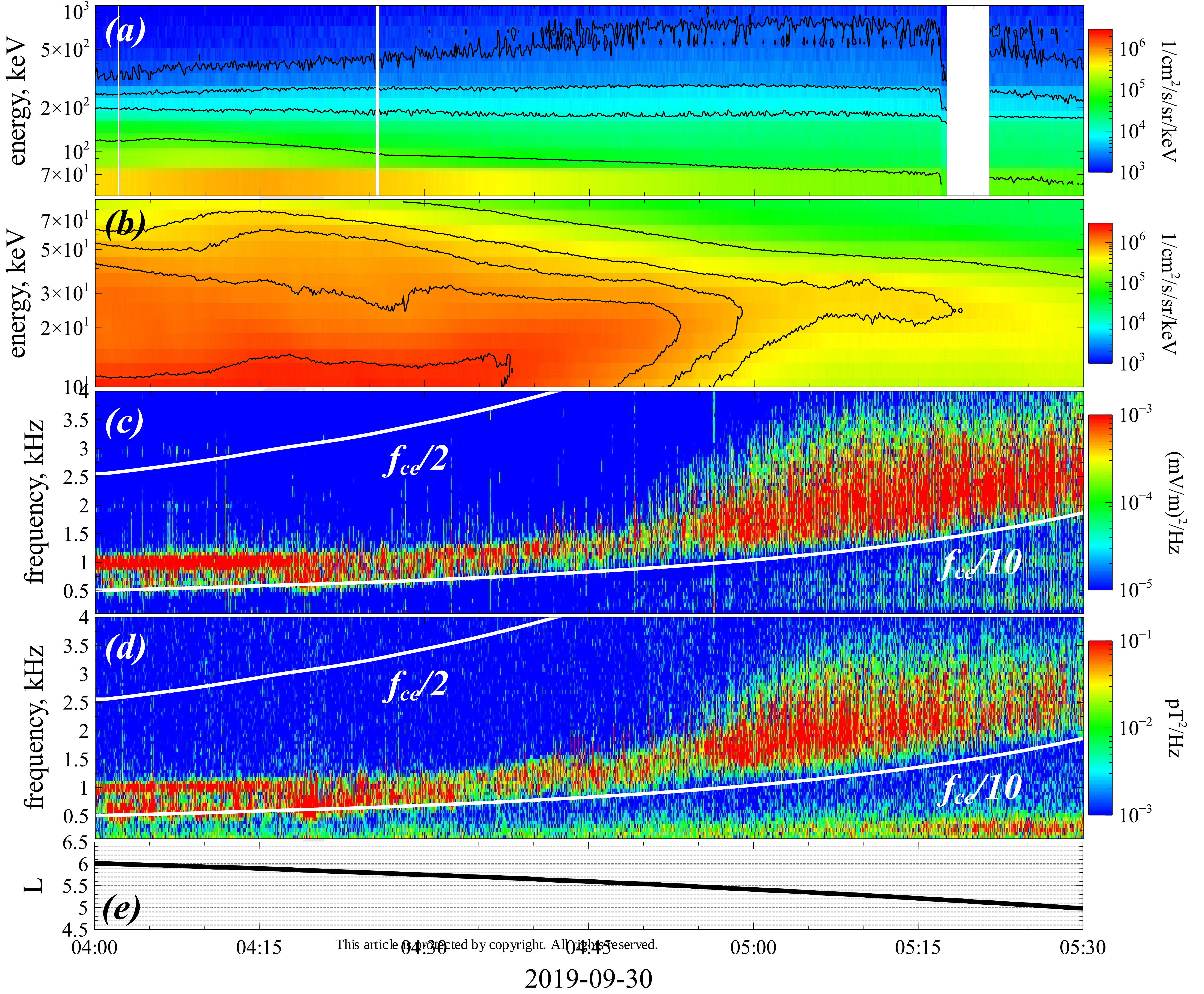

(a)
(b)
(c)
(d)
(e)
energy, keV
frequency, kHz
L
1/cm²/s/sr/keV
(mV/m)²/Hz
pT²/Hz
$f_{ce}/2$
$f_{ce}/10$
04:00
04:15
04:30
04:45
05:00
05:15
05:30
2019-09-30

Footprints 2019-09-30

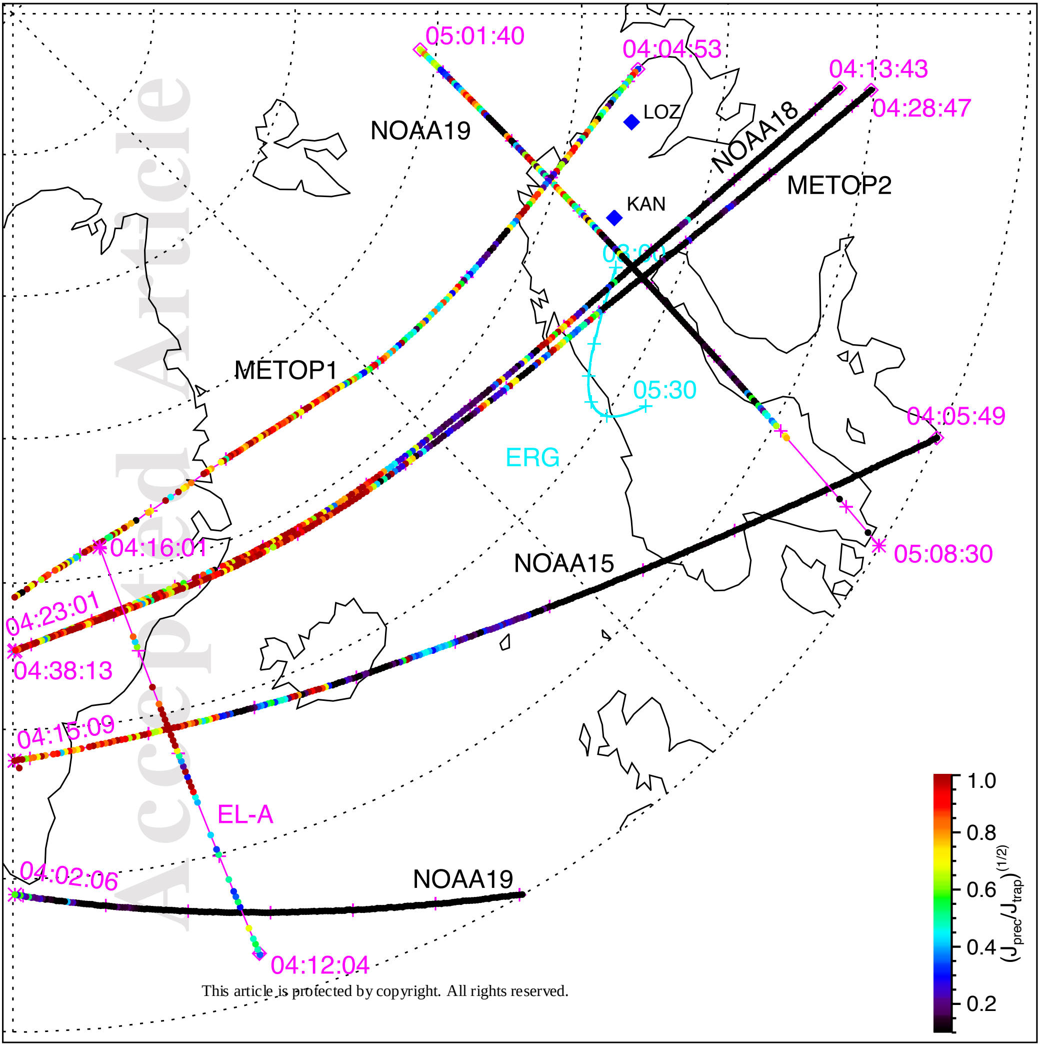

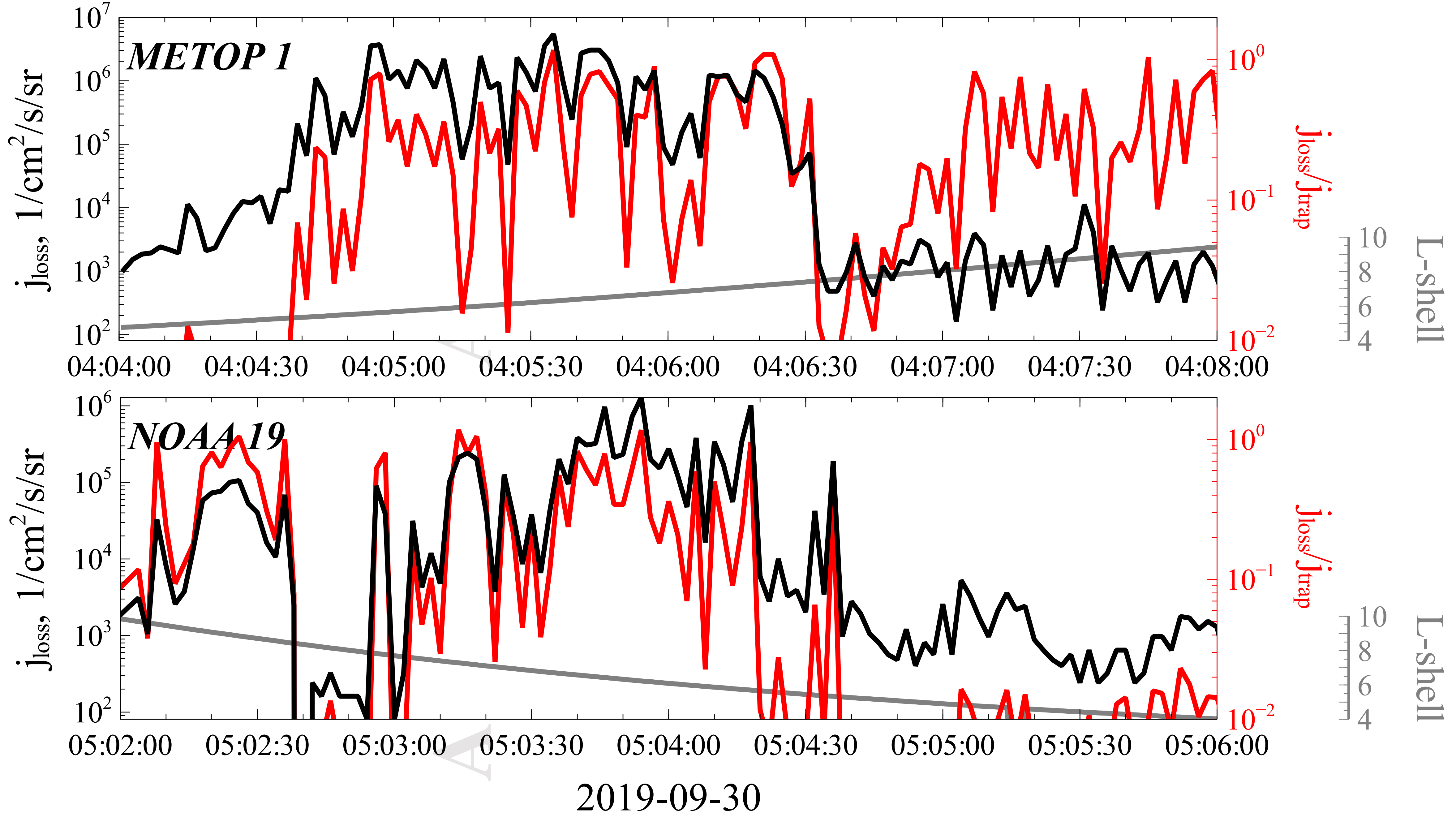
METOP 1
NOAA 19
j_{loss}, 1/cm^2/s/sr
j_{loss}/j_{trap}
L-shell
04:04:00
04:04:30
04:05:00
04:05:30
04:06:00
04:06:30
04:07:00
04:07:30
04:08:00
05:02:00
05:02:30
05:03:00
05:03:30
05:04:00
05:04:30
05:05:00
05:05:30
05:06:00
2019-09-30

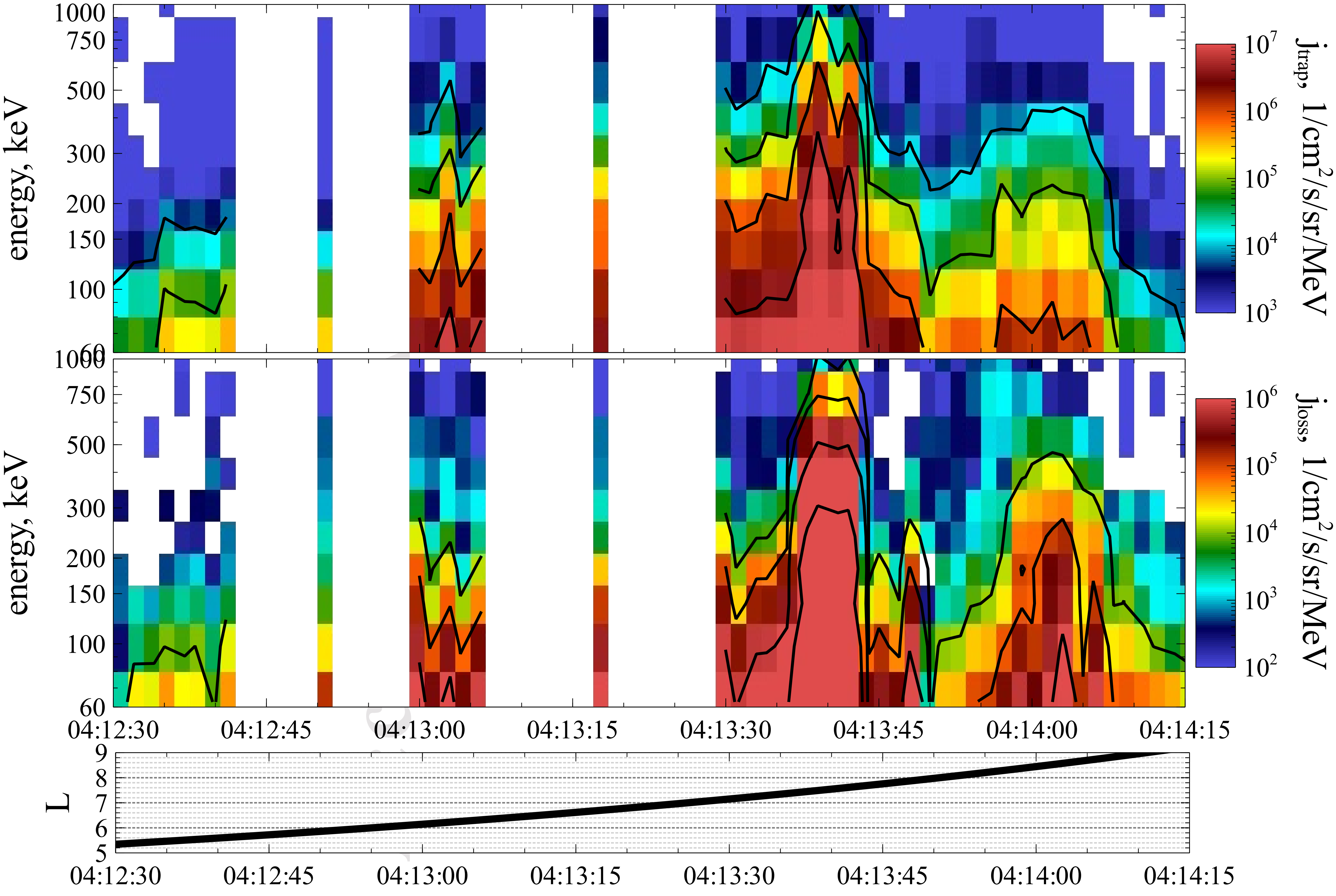

2019-09-30, ELFIN A

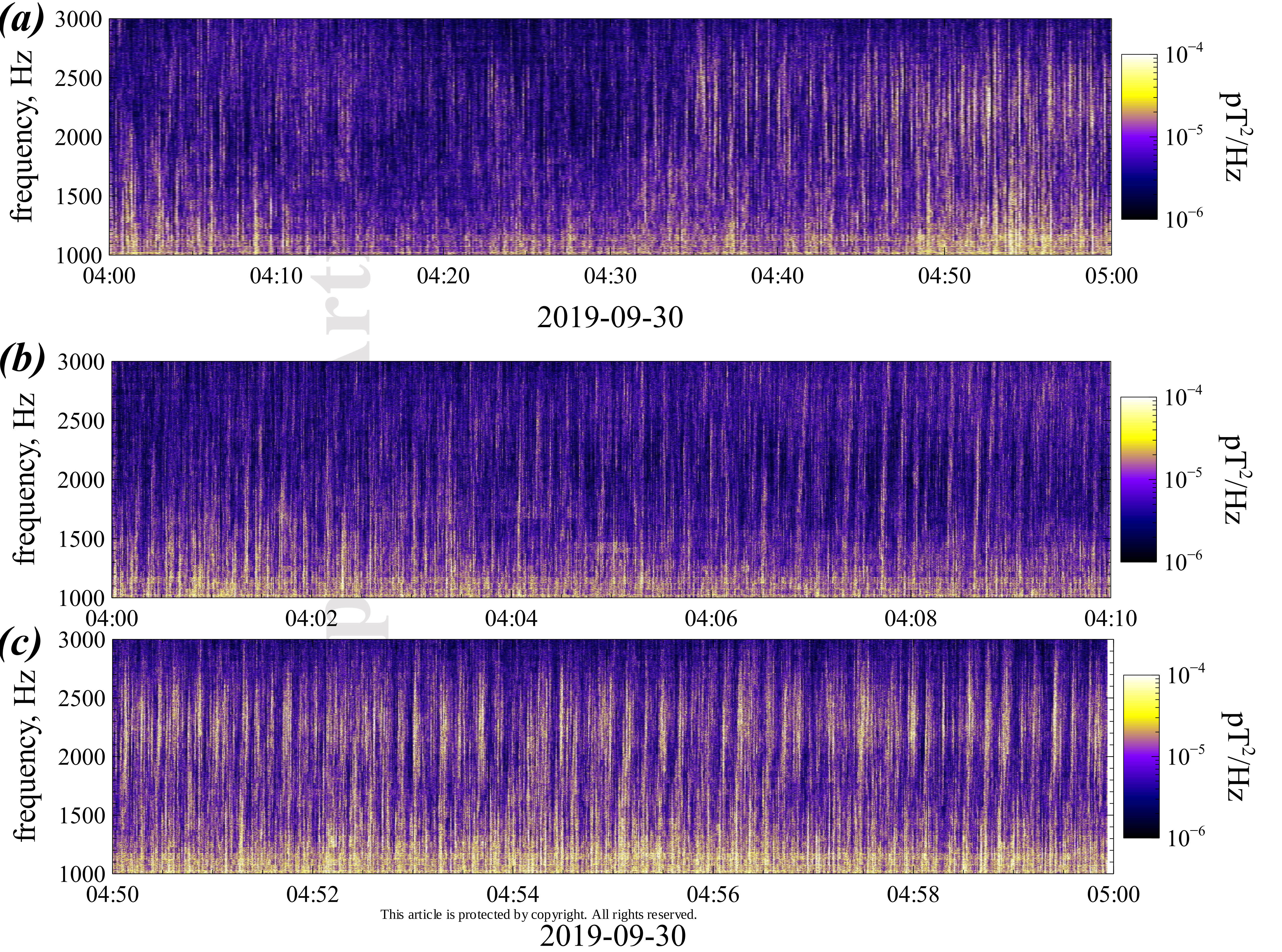
(a)
frequency, Hz
3000
2500
2000
1500
1000
04:00
04:10
04:20
04:30
04:40
04:50
05:00
2019-09-30
10−4
10−5
10−6
pT2/Hz
(b)
frequency, Hz
04:00
04:02
04:04
04:06
04:08
04:10
(c)
frequency, Hz
04:50
04:52
04:54
04:56
04:58
05:00
2019-09-30

Footprints 2019-10-06

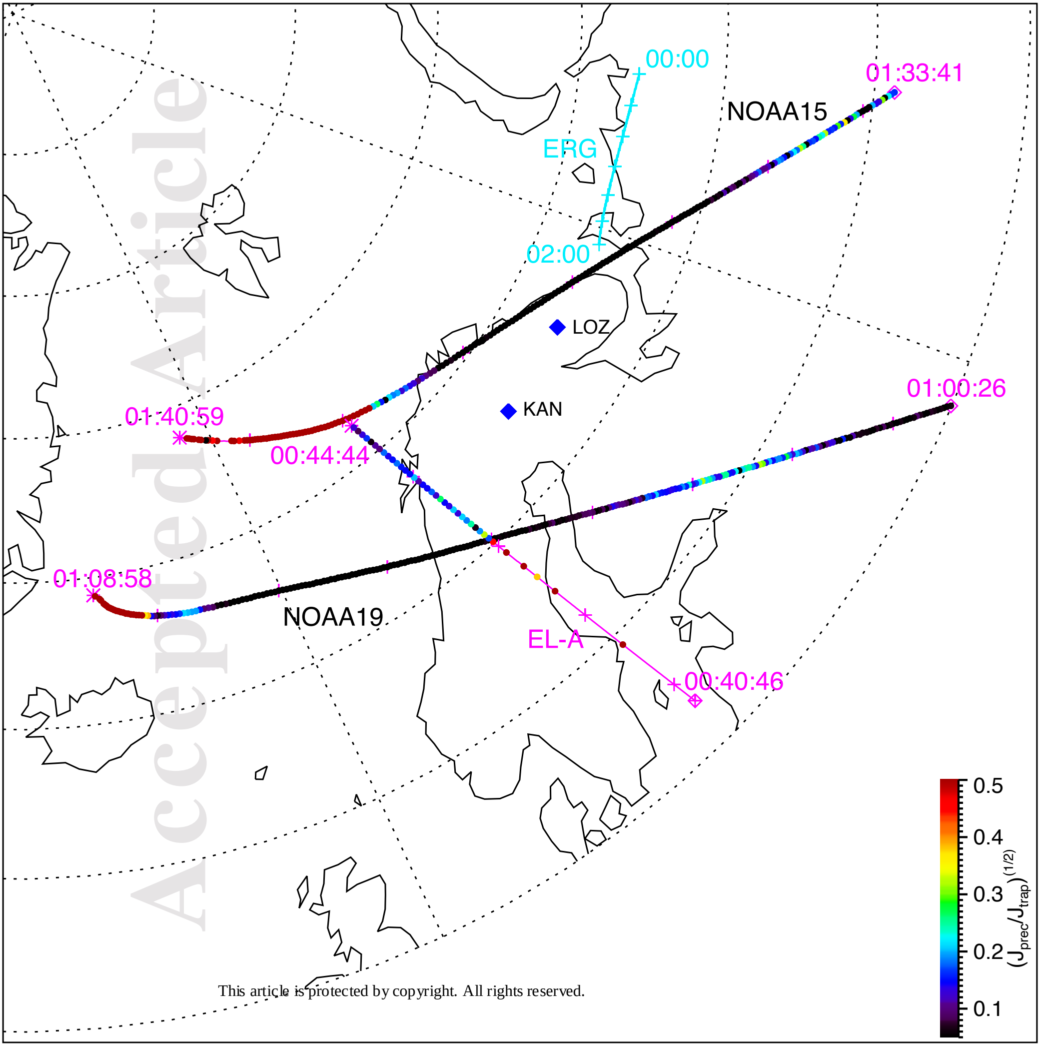

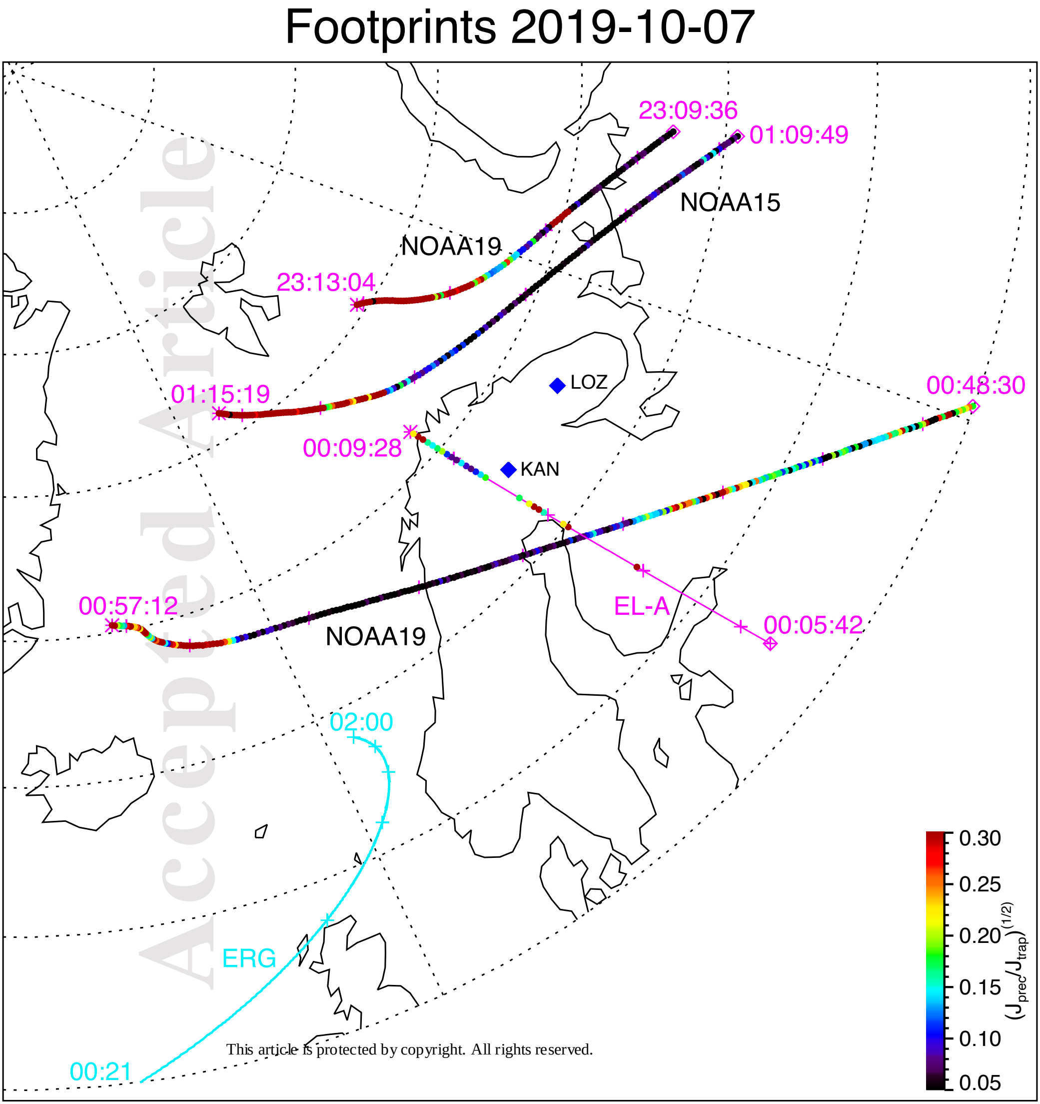
Footprints 2019-10-07
23:09:36
01:09:49
NOAA15
NOAA19
23:13:04
LOZ
01:15:19
00:48:30
00:09:28
KAN
EL-A
00:57:12
00:05:42
NOAA19
02:00
ERG
00:21
0.30
0.25
0.20
0.15
0.10
0.05
$(J_{prec}/J_{trap})^{(1/2)}$

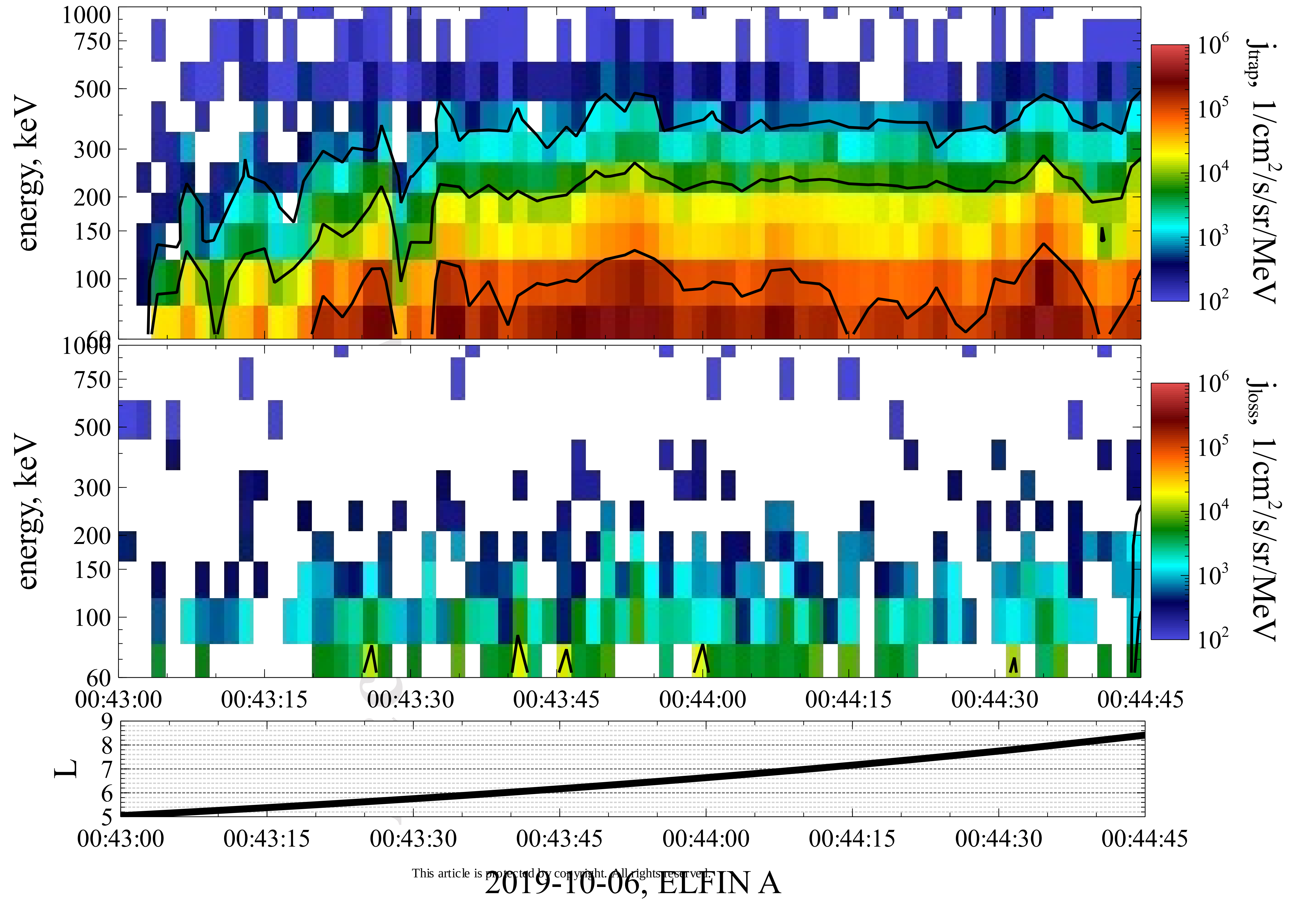

energy, keV
1000
750
500
300
200
150
100
60
j_trap, 1/cm²/s/sr/MeV
10⁶
10⁵
10⁴
10³
10²
j_loss, 1/cm²/s/sr/MeV
00:43:00
00:43:15
00:43:30
00:43:45
00:44:00
00:44:15
00:44:30
00:44:45
L
9
8
7
6
5
2019-10-06, ELFIN A

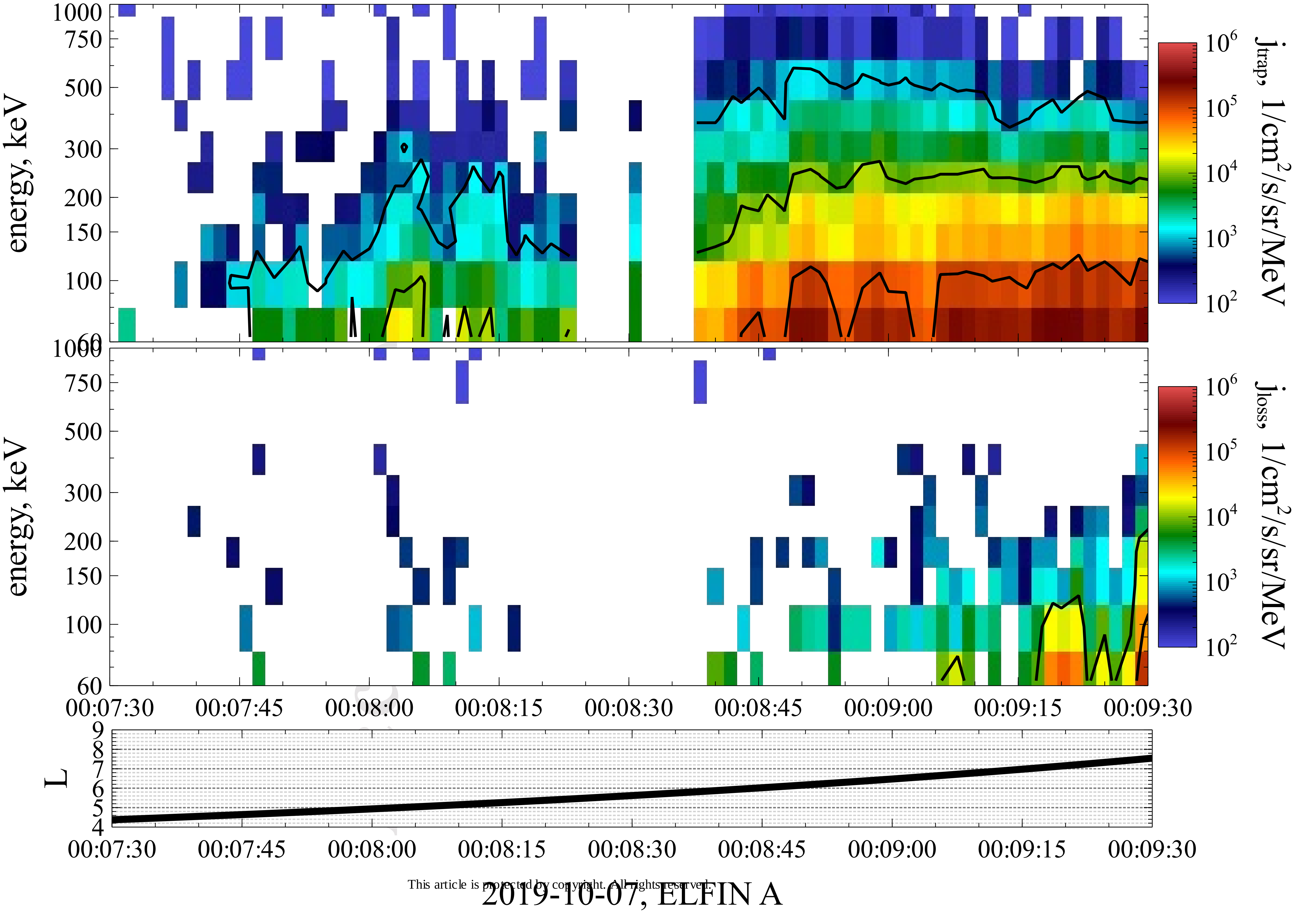

1000
750
500
300
200
150
100
60
energy, keV
j_trap, 1/cm²/s/sr/MeV
10⁶
10⁵
10⁴
10³
10²
j_loss, 1/cm²/s/sr/MeV
L
9
8
7
6
5
4
00:07:30
00:07:45
00:08:00
00:08:15
00:08:30
00:08:45
00:09:00
00:09:15
00:09:30
2019-10-07, ELFIN A